HHS Public Access

Author manuscript

Nat Immunol. Author manuscript; available in PMC 2021 February 10.

Published in final edited form as:

Nat Immunol. 2020 October ; 21(10): 1219–1231. doi:10.1038/s41590-020-0750-1.

IL-1 induces mitochondrial translocation of IRAK2 to suppress oxidative metabolism in adipocytes

Hao Zhou[1,10], **Han Wang**[1,2,10], **Minjia Yu**[1,3,10], **Rebecca C. Schugar**[4], **Wen Qian**[1], **Fangqiang Tang**[1], **Weiwei Liu**[1], **Hui Yang**[1], **Ruth E. McDowell**[1], **Junjie Zhao**[1], **Ji Gao**[5], **Ashok Dongre**[5], **Julie A. Carman**[5,9], **Mei Yin**[6], **Judith A. Drazba**[6], **Robert Dent**[7], **Christopher Hine**[4], **Yeong-Renn Chen**[8], **Jonathan D. Smith**[4], **Paul L. Fox**[4], **J. Mark Brown**[4], **Xiaoxia Li**[1,11]

[1]Department of Inflammation and Immunity, Lerner Research Institute, Cleveland Clinic, Cleveland, OH, 44195, USA.

[2]School of Life Sciences, Lanzhou University, Lanzhou, Gansu, 730000, China

[3]Department of Medicine, Mount Auburn Hospital, Harvard Medical School, Cambridge, MA, 02138, USA.

[4]Department of Cardiovascular & Metabolic Sciences, Lerner Research Institute, Cleveland Clinic, Cleveland, OH, 44195, USA.

[5]Discovery Biology, Bristol-Myers Squibb, Princeton, NJ, 08540, USA.

[6]Imaging Core, Lerner Research Institute, Cleveland Clinic, Cleveland, OH, 44195, USA.

[7]University of Ottawa and Ottawa Hospital, Ottawa, ON, K1H 8L6, Canada.

[8]Department of Integrative Medical Sciences, College of Medicine, Northeast Ohio Medical University, Rootstown, OH 44272, USA.

Abstract

Chronic inflammation is a common feature of obesity with elevated cytokines such as Interleukin-1 (IL-1) in circulation and tissues. Here, we report an unconventional IL-1R-MyD88-IRAK2-PHB/OPA1 signaling axis that reprograms mitochondrial metabolism in adipocytes to exacerbate obesity. IL-1 induced recruitment of IRAK2-Myddosome to mitochondria outer membrane via recognition by TOM20, followed by TIMM50-guided translocation of IRAK2 into mitochondria inner membrane to suppress oxidative phosphorylation and fatty acid oxidation, thereby, attenuating energy expenditure. Adipocyte-specific MyD88 or IRAK2 deficiency reduced high fat diet (HFD)-induced weight gain, increased energy expenditure and ameliorated insulin

[11]Correspondence should be addressed to X. L. (lix@ccf.org).

Author Contributions

H.Z, H.W, M.Y, R.C.S, W.Q, F.T, W.L, H.Y, R.E.M, & J.Z conducted the experiments. J.A.C., J.G. & A.D performed the proteomic analysis. R.D collected human adipose tissue samples. M.Y & J.A.D did the electron microscopy analysis. H.Z and X.L. wrote the manuscript. C.H, Y-R.C, J.D.S, P.L.F, J.M.B. and X.L. supervised the study.

[9]Current address: Immunology Discovery, Janssen Research and Development, Spring House, PA, 19477, USA

[10]These authors contributed equally to this work.

Competing Interests Statement

The authors declare no competing interests.

resistance, associated with a smaller adipocyte size and increased cristae formation. IRAK2 kinase inactivation also reduced HFD-induced metabolic diseases. Mechanistically, IRAK2 suppressed respiratory super-complex formation via interaction with PHB1 and OPA1 upon stimulation of IL-1. Taken together, our results suggest that IRAK2 Myddosome functions as a critical link between inflammation and metabolism, representing a novel therapeutic target for patients with obesity.

Introduction

Obesity is an increasing global problem with severe clinical consequences, including Type 2 diabetes, metabolic syndrome, premature aging and cancer[1, 2, 3]. Emerging evidence has suggested that adipose tissue dysfunction is a critical component of the obesity-associated pathologies contributing to metabolic syndromes[4, 5, 6, 7]. Notably, adipocytes in adipose tissue are not simply a passive fat storing depot, but rather constituents of a dynamic endocrine organ majorly contributing to metabolic control and adipose tissue homeostasis[8]. High fat diet (HFD) induces the accumulation of endogenous ligands of Toll-like receptors (TLRs, including free fatty acids (FFAs), oxidized low density lipoprotein (ox-LDL), and inflammatory cytokines such as Interleukin-1β (IL-1β)[9, 10, 11, 12, 13, 14]. TLR/interleukin-1 receptor (IL-1R) signaling plays an important role in HFD-induced adipose tissue dysfunction[15, 16, 17, 18, 19]. While TLRs and IL-1R are highly expressed in adipocytes, the mechanism and pathophysiological importance of TLR/IL-1R signaling in adipocytes during obesity-induced adipose tissue inflammation remain unclear.

TLR/IL-1R transduce signals through the adaptor molecule MyD88 and IL-1R-associated kinase (IRAK) family members, including IRAK1, IRAK2, IRAKM and IRAK4[20]. IRAK4 is the upstream kinase of IRAK1 and IRAK2[21]. TLR/IL-1R activation leads to the formation of Myddosome complexes (MyD88-IRAK4-IRAK1; MyD88-IRAK4-IRAK2). While IRAK1 mediates TAK1-dependent NFκB activation[22], IRAK2 is critical for posttranscriptional control[23, 24]. We previously reported that deficiency of MyD88 in myeloid cells prevented macrophage recruitment to adipose tissue and their switch to an M1-like phenotype, accompanied by substantially reduced diet-induced systemic inflammation and insulin resistance[25]. In addition to inflammatory responses, recent studies have shown the critical impact of TLR/IL-1R on cell metabolism, including glycolysis and lipid accumulation[26, 27, 28, 29]. However, the molecular mechanisms for how TLR/IL-1R signaling modulates cell metabolism and the impact on obesity-induced metabolic syndrome are the critical questions in this emerging field.

Here we show that adipocyte-specific deficiency of MyD88 or IRAK2 reduces diet-induced weight gain associated with a smaller adipocyte size, increased body energy expenditure and improves insulin resistance. Mechanistically, we have discovered an unconventional IL-1R-MyD88-IRAK2-PHB/OPA1 signaling axis that directly impacts on adipocyte metabolism contributing to obesity. We showed that IL-1 stimulation induced the translocation of IRAK2 Myddosome to mitochondria outer membrane via recognition by TOM20, followed by TIMM50-guided translocation of IRAK2 into mitochondria inner membrane. IRAK2 then interacts with mitochondria proteins [Prohibitin (PHB) and Optic Atrophy Protein 1

(OPA1)], resulting in suppression of respiratory super-complex formation, oxidative phosphorylation (OxPhos) and fatty acid β-oxidation (FAO). While the PHB-OPA1 interaction is substantially reduced in IRAK2 deficient and IRAK2 kinase-inactive knockin (IRAK2 KI) adipocytes, IRAK2 deficiency or kinase inactivation reduces HFD-induced metabolic diseases. These results suggest that TLR/IL-1R-MyD88 signaling reprograms cell metabolism in adipocytes, contributing to diet-induced adipose tissue dysfunction and obesity.

Results

IL-1β inhibits OxPhos and super-complex formation

Previous studies have shown that HFD induces low-grade inflammation and accumulation of cytokines such as IL-1 in circulation and tissues[6, 11, 30, 31, 32]. We detected elevated *Il1b* mRNA expression in the human adipose tissue from diabetic patients compared to that of non-diabetic individuals (Fig. 1a), in agreement with previous reports[33]. Patient demographics and clinical characteristics are provided in Extended Data Fig. Fig. 1a. IL-1β production was much higher in epididymal white adipose tissue (eWAT), inguinal white adipose tissue (iWAT) and brown adipose tissue (BAT) from HFD-fed mice (Fig. 1b,c). Therefore, we hypothesized that IL-1R signaling might have a direct impact on adipocyte cell metabolism. We found that IL-1β stimulation suppressed OxPhos with increased the extracellular acidification rate (ECAR) in adipocytes analyzed by extracellular flux analysis (Fig. 1d & Extended Data Fig. Fig. 1b). Mitochondrial respiratory complexes (I-IV) drive OxPhos by sustaining a proton-motive force across the inner membrane that is used to synthesize ATP, which can be organized into super-complexes to promote cellular respiration[34]. Importantly, we found that IL-1β suppressed super-complex formation in adipocytes (Fig. 1e & Extended Data Fig. Fig. 1c), while the protein levels of each individual complex were not affected by IL-1β stimulation (Extended Data Fig. Fig. 1d). In support of this observation, we found that the enzymatic activity of the super-complex (I +III) was severely decreased in IL-1β-treated adipocytes compared to the untreated cells, whereas IL-1β treatment only slightly suppressed individual Complex I and Complex III activity (Fig. 1f). Consistently, the cellular ATP level, ATP-linked oxygen consumption (OCR) and FAO rate were substantially reduced in IL-1β-stimulated wild-type adipocytes, but not in IL-1R knockout cells (Fig. 1d,g,h & Extended Data Fig. Fig. 1e). Conversely, IL-1β stimulation did not increase cytosolic mtDNA, calcium and cytochrome C levels (Extended Data Fig. Fig. 2a–c). Cellular reactive oxygen species (ROS) and mitophagy activation were not affected by IL-1β stimulation (Extended Data Fig. Fig. 2d,e). Taken together, these results indicate a critical role of IL-1β in adipocyte metabolism by specifically inhibiting mitochondrial oxidative function and super-complex formation.

Myd88^{AKO} improves obesity and energy expenditure

The adapter molecule MyD88 is recruited to TLR and IL-1R complexes upon ligand stimulation[35]. Our previous study suggested that myeloid MyD88 is critical for HFD-induced switching of adipose tissue macrophages from M2-like macrophages to M1-like macrophages[25]. We have recently generated adipocyte-specific MyD88-deficient (*Myd88*^{AKO}) mice by breeding *Myd88*$^{fl/fl}$ (*Myd88*^{FF}) mice to Adiponectin-Cre transgenic

mice. The deletion efficiency was validated by immuno-blot analysis in eWAT, iWAT and BAT tissue lysates (Extended Data Fig. Fig. 3a). There were no detectable differences between 6-weeks old *Myd88*^{AKO} and littermate control mice in their body weight, adipocyte differentiation (as assessed by gene expression) and adipose tissue weight (data not shown). *Myd88*^{AKO} male mice and gender-matched littermate controls (*Myd88*^{FF}) were then subjected to HFD for 12 weeks and monitored for weight changes on a weekly basis. Compared to wild-type control mice, *Myd88*^{AKO} mice gained less weight and exhibited improved glucose tolerance and insulin sensitivity (Fig. 2a,b). Adipocyte cell sizes were decreased in iWAT of *Myd88*^{AKO} mice compared to wild-type littermate control mice (Fig. 2c). HFD-induced formation of crown-like structure and inflammatory gene expression were reduced in iWAT of *Myd88*^{AKO} mice compared to control mice (Fig. 2d,e). Furthermore, there was an increase in cristae formation of iWAT from *Myd88*^{AKO} mice compared to that in control mice, which was accompanied by elevated thermogenic gene expression including *Ucp1* (Fig. 2e & Extended Data Fig. Fig. 3b).

We next examined the impact of adipocyte-specific MyD88 deficiency on energy expenditure. Interestingly, HFD-fed *Myd88*^{AKO} mice had an increased energy expenditure at both 22 °C and 4 °C compared to control mice (Fig. 2f). Notably, *Myd88*^{AKO} BAT had much reduced lipid accumulation with increased thermogenic gene expression, including *Ucp1*, *Prdm16* and *Pgc1a*, compared to control mice (Fig. 2g). Electron microscopy showed that cristae structure was better organized in *Myd88*^{AKO} BAT (Fig. 2h), accompanied by increased mitochondrial respiratory super-complex formation (Fig. 2i). Consistently, the super-complex (I+III) activity (but not individual Complex I or III) was substantially increased in the mitochondria isolated from *Myd88*^{AKO} BAT compared to that from wild-type BAT (Fig. 2j). Moreover, *Myd88*^{AKO} BAT displayed higher FAO capacity than the control BAT (Fig. 2k & Extended Data Fig. Fig. 3d). Taken together, these results suggest that adipocyte-derived MyD88 might play an important role in driving HFD-induced BAT dysfunction by interfering with mitochondrial function.

Translocation of IRAK2 into inner mitochondrial membrane

Leveraging subcellular fractionation, we indeed found that IL-1β stimulation was able to induce translocation of MyD88, IRAK4 with IRAK2, but not IRAK1, to mitochondria (Fig. 3a). Sub-mitochondrial fractionation analysis indicates that only IRAK2 was translocated into the mitochondrial intermembrane space and inner membrane (Fig. 3b). In contrast, MyD88 and IRAK4 were only found in the outer membrane fraction (Fig. 3b). Interestingly, immuno-blot analysis showed majority of IRAK2 was modified in mitochondrial fraction which can be removed by phosphatase treatment, suggesting that IRAK2 was phosphorylated in mitochondria (Extended Data Fig. Fig. 4a). To visualize mitochondrial IRAK2, we generated HA-tagged IRAK2 reporter mouse by inserting three HA tags at the C-terminal of *Irak2* (Extended Data Fig. Fig. 4b). Importantly, we detected HA-IRAK2 in the mitochondria by immunogold staining in IL-1β-treated primary adipocytes derived from iWAT of HA-*Irak2* knockin mice (Fig. 3c). Furthermore, HA-tagged IRAK2 was expressed in IL-1R1 deficient and MyD88 deficient adipocytes, followed by immunogold staining and electron microscopy analysis. IRAK2 mitochondrial localization was greatly reduced in IL-1-treated IL-1R1 deficient and MyD88 deficient adipocytes, suggesting that IRAK2

mitochondrial localization was dependent on IL-1-mediated signaling activation (Extended Data Fig. Fig. 4c). We also generated HA-tagged MyD88 reporter mice by inserting three HA tags at the C-terminal of *Myd88*. By immunogold staining, we found that MyD88 localized around the edge of mitochondria structure in IL-1β-treated primary adipocytes (Extended Data Fig. Fig. 4d), supporting the localization of MyD88 on the outer membrane from the sub-mitochondrial fractionation analysis (Fig. 3b). Taken together, these results allow us to propose the following model: IL-1β stimulation leads to MyD88/IRAK4/IRAK2 Myddosome complex formation and translocation to the outer mitochondrial membrane where IRAK2 may then dissociate from the complex and translocate into mitochondrial intermembrane space and inner membrane. In support of this model, through mass spectrometric analysis of IRAK2 interacting proteins, we found that IRAK2 was able to interact with TOM20 and TIMM50 which are translocators on mitochondrial outer and inner membrane respectively[36, 37, 38]. We validated IL-1β-induced IRAK2's interaction with TOM20 and TIMM50 by co-immunoprecipitation. (Extended Data Fig. Fig. 4e).

Consistent with the mitochondrial translocation of IRAK2 Myddosome, IRAK2 deficiency ablated IL-1β-induced suppression on super-complex formation of respiratory chain (Fig. 3d & Extended Data Fig. Fig. 5a) and the enzymatic activity of the super-complex (I+III) (Fig. 3e). Furthermore, while IL-1β-induced inflammatory gene expression was not affected in IRAK2-deficient adipocytes (Extended Data Fig. 5b), IRAK2 deficiency abolished IL-1-induced inhibition of OxPhos with minimum impact on ECAR (Fig. 3f & Extended Data Fig. 5c), cellular ATP levels (Fig. 3g) and FAO (Fig. 3h & Extended Data Fig. 5d). Our data suggest IRAK2 might suppress OxPhos by directly disrupting mitochondrial respiratory chain super-complex formation in the mitochondria. TOM20 is the major receptor responsible for the recognition and translocation of cytosolically synthesized proteins. Nuclear magnetic resonance (NMR) and crystal structures of the TOM20 receptor domain demonstrated that TOM20 recognizes the hydrophobic surface of the presequence amphipathic helix[38, 39, 40]. IRAK2 contains an amphipathic helix structure at its N-terminal (Extended Data Fig. 5e). Mutation of the positively charged amino acids in mitochondria localization signal (MLS) in IRAK2 (IRAK2$^{Mito\text{-}mut}$, R43A/K44A/K46A/R50A) greatly reduced the interaction of IRAK2 with TOM20 and diminished IRAK2 mitochondria localization (Fig. 3i–j). IRAK2$^{Mito\text{-}mut}$ attenuated the impact of IRAK2 on super-complex formation, enzymatic activity of the super-complex (I+III), cellular ATP level, ATP-linked OCR and FAO rate in adipocytes (Fig. 3k–n & Extended Data Fig. 5f,g). Taken together, these data suggest that IL-1β-stimulation induces IRAK2 mitochondrial translocation, thereby inhibiting OxPhos and FAO.

IRAK2 deficiency improves HFD-induced obesity

To investigate the role of IRAK2 in HFD-induced metabolic diseases, IRAK2-deficient male mice and gender-matched littermate controls were subjected to HFD for 12 weeks and monitored for weight changes on a weekly basis. Compared to wild-type control mice, IRAK2-deficient mice gained less weight in response to HFD feeding (Fig. 4a). We quantified the weight of each organ as a percentage of whole-body weight, and found only eWAT and iWAT showed reduced weight in IRAK2-deficient mice (Fig. 4b). EchoMRI analysis also indicated that IRAK2 deficiency reduced the fat mass in response to HFD

feeding (Fig. 4c). Additionally, IRAK2 deficiency attenuated the development of HFD-induced insulin resistance (Fig. 4d). Histological analysis showed that the adipocyte cell sizes were decreased in the iWAT of IRAK2-deficient mice compared to that in the wild-type littermate control mice (Fig. 4e). HFD-induced formation of crown-like structure was reduced in iWAT of IRAK2-deficient mice accompanied by reduced inflammatory gene expression (Fig. 4f,i). Furthermore, transmission electron microscopy analysis showed that mitochondrial cristae area was increased in adipocytes of IRAK2-deficient iWAT from HFD-fed mice (Fig. 4g). Consistently, there was increased FAO activity and elevated thermogenic gene expressions in IRAK2-deficient iWAT compared to control mice (Fig. 4h,i). Since type 2 diabetes is considered as a gender-associated disease[41, 42], IRAK2-deficient female mice and gender-matched littermate controls were also subjected to HFD for 12 weeks and monitored for weight changes on a weekly basis. Similar to male mice, HFD-fed IRAK2-deficient female mice reduced weight gain, improved insulin sensitivity, decreased adipocyte cell size with reduced lipid accumulation in adipose tissue, compared to the wild-type littermate control mice (Extended Data Fig. 6). These results suggest that IRAK2 deficiency rendered resistance to HFD-induced obesity.

IRAK2 deficiency prevents HFD-induced BAT dysfunction

BAT is critical for thermogenesis due to uncoupled mitochondrial respiration, implicated as an important site for modulating energy expenditure[43]. Importantly, IRAK2-deficient BAT showed much decreased lipid accumulation and increased FAO activity compared to that in control mice (Fig. 5a,b & Extended Data Fig. 7a). These results indicate that IRAK2 deficiency prevented HFD-induced BAT dysfunction. Immunogold staining of HA-tagged IRAK2 clearly indicated IRAK2 expression in the mitochondria in the BAT from obese mice (Fig. 5c & Extended Data Fig. 7b), suggesting that mitochondrial IRAK2 might contribute to HFD-induced BAT dysfunction. Electron microscopy analysis showed that cristae area was increased in IRAK2-deficient BAT, accompanied by increased super-complex formation in BAT and compared to that in control mice after HFD (Fig. 5d,e & Extended Data Fig. 7c). Analysis of respiratory complexes enzymatic activities indicated slightly Complex I and Complex III activities and greatly increased activity of the super-complex (I+III) was detected in the mitochondria isolated from IRAK2-deficient BAT (Fig. 5f).

We then examined the impact of IRAK2 deficiency on thermogenesis and energy expenditure. HFD-fed IRAK2-deficient mice had an increased energy expenditure at 4 °C compared to that of control mice (Fig. 5g). IRAK2-deficient BAT showed relative increased expression of these thermogenic genes under HFD compared to their levels in control mice (Fig. 5h). Moreover, HFD-fed IRAK2-deficient mice displayed higher body temperature compared to the control mice under HFD (Fig. 5i). Consistently, HFD-fed *Myd88*^{AKO} mice also displayed higher body temperature compared to the control mice (Extended Data Fig. 3e). We then used Ucp1 reporter mice (Ucp1-luc/tdTomato) to monitor the thermogenic function of BAT *in vivo* by breeding IRAK2-deficient mice onto Ucp1-luc, tdTomato reporter mice. Both luciferase activity and RFP signal were increased in the BAT (and iWAT) from IRAK2-deficient mice compared to control mice under HFD (Extended Data Fig. 7 d,e). IRAK2 deficiency also increased Ucp-1-driven luciferase activity and RFP signal in the BAT (and iWAT) in response to β-adrenergic receptor agonist CL-316,274 (Extended

Data Fig. 7 f,g). These results suggest that IRAK2 suppresses mitochondrial function by inhibiting super-complex formation and uncoupled mitochondria respiration in BAT, contributing to the decreased energy expenditure.

IRAK2 disrupts super-complex formation via PHB-OPA1

We next investigated the molecular mechanism for how IRAK2 inhibits mitochondrial respiratory chain super-complex formation. Our proteomic analysis of IRAK2-interacting proteins revealed that IRAK2 interacts with mitochondrial protein PHB. PHB was shown to play a critical role in mitochondrial function and required for adipocyte differentiation[44]. We found IL-1β stimulation induced the interaction between IRAK2 and PHB, but not PHB2, using mitochondrial fractionation of primary adipocytes (Fig. 6a & Extended Data Fig. 8a). Interestingly, IL-1β stimulation also induced the interaction of IRAK2 and PHB with OPA1 (Fig. 6a & Extended Data Fig. 8a), a dynamin-related protein that helps to tighten the cristae junctions for super-complex stability[45, 46]. Notably, while IL-1β-induced PHB-OPA1 interaction was significantly reduced in IRAK2-deficient adipocytes (Fig. 6a & Extended Data Fig. 8b), PHB knockdown reduced IL-1β-induced interaction of IRAK2 with OPA1 (Fig. 6b and Extended Data Fig. 8c). These results suggest that IRAK2 suppresses super-complex formation via interaction with the PHB-OPA1 axis. In support of this finding, the impact of IRAK2 on IL-1β-induced suppression of mitochondrial function (including super-complex formation and FAO) disappeared in PHB knockdown cells (Extended Data Fig. 8d–h). Furthermore, PHB overexpression promoted super-complex activity and FAO rate in in WT and IRAK2-deficient primary adipocytes. IL-1β treatment suppressed super-complex activity and FAO rate PHB overexpressed cells, but not in PHB overexpressed IRAK2-deficient adipocytes (Extended Data Fig. 8i,j). Taken together, these data suggest that the suppression effect of IL-1-IRAK2 signaling axis on mitochondrial super-complex activity and FAO rate in adipocytes is dependent on PHB.

IRAK2 kinase inactivation impaired IL-1β-induced IRAK2 modification and the interaction of IRAK2 with PHB-OPA1, although IL-1β was still able to drive IRAK2-kinase inactive mutant (IRAK2 KI) into mitochondria (Fig. 6c and Extended Data Fig. 9a). IRAK2 kinase inactivation abolished IL-1β-induced suppression of mitochondrial super-complex formation (Fig. 6d & Extended Fig. 9b), enzymatic activity of the super-complex (I+III) (Fig. 6e), cellular ATP level (Fig. 6f), ATP-linked OCR and OxPhos (Fig. 6g & Extended Data Fig. 9c), and FAO (Fig. 6h and Extended Data Fig. 9d). Notably, while the kinase-inactive IRAK2 in the mitochondria lost the ability to interact with PHB-OPA1, there was also the loss of IL-1β-induced IRAK2 modification (Fig. 6c), implicating that IRAK2 auto-phosphorylation might be important for the interaction of IRAK2 with PHB-OPA1. On the other hand, IRAK2 is known be phosphorylated at serine 134 (S134) and threonine 140 (T140) upon activation of TLR activation[24]. Mutation of S134 and T140 (IRAK2 phospho^{Mut}, S136A/T140A) abolished IL-1β-induced IRAK2 modification in mitochondria (Fig. 6i) and its interaction with TIMM50 (but not TOM20) and PHB-OPA1 (Fig. 6j). Taken together, these data suggest that IRAK2 auto-phosphorylation is required for TIMM50-guided localization of IRAK2 on mitochondrial inner membrane to interact with PHB-OPA1.

IRAK2 kinase-inactivation and IRAK2^{AKO} improves obesity

We then examined the role of IRAK2 kinase activity in HFD-induced obesity. Similar to IRAK2-deficient mice, IRAK2 kinase-inactive gene-targeted mice (*Irak2* KI) gained less weight and had reduced insulin resistance compared to the wild-type control mice under HFD (Fig. 7a,b). Furthermore, HFD-fed *Irak2* KI mice exhibited increased energy expenditure at 4 °C (Fig. 7c) and displayed increased body temperature (Extended Data Fig. 10a) compared to control mice. Histological analysis showed that the adipocyte cell sizes were decreased in the iWAT of *Irak2* KI mice compared to control mice (Fig. 7d). Moreover, *Irak2* KI BAT had much reduced lipid accumulation with increased thermogenic gene expression, compared to that in control mice (Fig. 7e,f). Consistently, HFD-fed *Irak2* KI mice showed increased mitochondrial super-complex formation (Fig. 7g & Extended Data Fig. 10b), increased activity of the super-complex (I+III) in BAT (Fig. 7h) and increased FAO capacity (Fig. 7i).

To further study role of IRAK2 in adipocyte in HFD-induced obesity. We have recently generated IRAK2 conditionally deficient mice by flanking exon 1 of *Irak2* by *lox*P sites (*Irak2*^{FF} mice) (Extended Data Fig. 10c). Adipocyte-specific IRAK2-deficient (*Irak2*^{AKO}) mice were generated by breeding *Irak2*^{FF} mice to Adiponectin-Cre transgenic mice. The deletion efficiency was validated by immuno-blot analysis in both iWAT and BAT tissue lysates (Extended Data Fig. 10d). Similar to IRAK2-deficient mice and *Irak2* KI mice, *Irak2*^{AKO} gained less weight and had reduced insulin resistance compared to the wild-type control mice under HFD (Fig. 8a,b), accompanied with increased body temperature (Extended Data Fig. 10e). Furthermore, HFD-fed *Irak2*^{AKO} mice exhibited increased energy expenditure compared to control mice (Fig. 8c). Histological analysis showed that the adipocyte cell sizes were decreased in the iWAT of *Irak2*^{AKO} mice compared to control mice (Fig. 8d). Moreover, *Irak2*^{AKO} BAT had much reduced lipid accumulation with increased thermogenic gene expression, including *Ucp1*, *Prdm16* and *Pgc1a*, compared to that in control mice (Fig. 8e,f). Consistently, HFD-fed *Irak2*^{AKO} mice showed increased mitochondrial super-complex formation (Fig. 8g & Extended Data Fig. 10f), increased activity of the super-complex (I+III) in BAT (Fig. 8h) and increased FAO capacity (Fig. 8i). These results suggest that IRAK2 kinase activity in adipocytes contributes HFD-induced obesity and BAT dysfunction.

Discussion

We report here that IL-1R signaling reprograms mitochondrial metabolism in adipocytes to attenuate energy expenditure by driving the recruitment of IRAK2 Myddosome to mitochondria outer membrane via recognition by TOM20, followed by TIMM50-guided translocation of IRAK2 into mitochondria inner membrane, resulting in suppression of respiratory super-complex formation, OxPhos and FAO. In response to IL-1β stimulation, IRAK2, but not kinase-inactive mutant, suppressed respiratory super-complex formation via interaction with mitochondrial proteins PHB and OPA1 in adipocytes. IRAK2 deficiency and kinase inactivation ablated IL-1β-induced PHB-OPA1 interaction in adipocytes and PHB knockdown abolished the regulatory role of IRAK2 in mitochondria. Taken together,

our results suggest that IRAK2 Myddosome mediates the IL-1R-MyD88-IRAK2-PHB/OPA1 signaling axis to directly impact on adipocyte metabolism and energy expenditure.

In support of the critical role of IRAK2 Myddosome in adipocyte metabolism, we found that adipocyte-specific deficiency of MyD88 or IRAK2 reduced diet-induced weight gain, increased whole body energy expenditure and ameliorated insulin resistance. Consistently, ablation of IRAK2 Myddosome resulted in smaller adipocytes with increased cristae formation in both WAT and BAT from HFD-fed mice, which is accompanied by increased fatty acid oxidation. In parallel, adipocyte-specific deficiency of MyD88 or IRAK2 reduced the weight gain of WAT and attenuated whitening of BAT in response to HFD.

Notably, HFD-fed IRAK2 deficient mice had an increased energy expenditure at 4 °C compared to that of control mice. Furthermore, IRAK2-deficient BAT showed much increased expression of thermogenic genes including Ucp1 and displayed higher body temperature compared to the control mice. Collectively, these results implicate a critical impact of IRAK2 deficiency on non-shivering thermogenesis. In support of this hypothesis, IRAK2 deficiency also increased Ucp-1-driven luciferase activity and RFP signal in the BAT in response to β-adrenergic receptor agonist CL-316,274. Adipocyte-specific deficiency of MyD88 showed an increased energy expenditure at both 22 °C and 4 °C compared to that of control mice, suggesting the possible involvement of additional metabolic pathways mediated by other IRAK Myddosomes. IRAK1 deficiency was shown to reduce HFD-induced metabolic disease[47]. Future studies are required to investigate the impact of MyD88-dependent IRAK2-independent pathways in energy expenditure and metabolic diseases.

One important question is what the molecular signal is that triggers MyD88/IRAK2 mitochondrial translocation. Although subcellular fractionation showed that IL-1β stimulation induced translocation of MyD88, IRAK4 with IRAK2 (but not IRAK1) into mitochondria fraction, sub-mitochondrial fractionation analysis indicates that only IRAK2 was translocated into the mitochondrial intermembrane space and localized on inner membrane. On the other hand, MyD88 and IRAK4 were only found in the outer membrane fraction. Consistently, immunogold staining showed that while IRAK2 is localized inside the mitochondria, MyD88 is detected around the edge of mitochondria structure. These results suggest that IL-1β stimulation leads to MyD88/IRAK4/IRAK2 complex formation and translocation to the outer mitochondrial membrane where IRAK2 may then dissociate from the complex and translocate into mitochondrial intermembrane space and inner membrane. In support of this model, IRAK2 interacts with TOM20 and TIMM50 which are translocators on mitochondrial outer and inner membrane respectively. We identified a mitochondria translocation signal (MLS, an amphipathic helix structure) at its N-terminal and mutation of the positive charged amino acids within MLS abolished IRAK2's interaction with TOM20 and impaired IRAK2's mitochondrial translocation. On the other hand, mutation of phosphorylation sites of IRAK2 abolished its interaction with TIMM50, but not TOM20, suggesting that IRAK2 auto-phosphorylation might serve as the molecular signal for its translocation into the mitochondrial inner membrane. Notably, MyD88 deficiency abolished IL-1β-induced mitochondria translocation of IRAK2 and the interaction of IRAK2 with TOM20 and TIMM50 in adipocytes (data not shown), suggesting

that IL-1β-induced Myddosome formation is required for the initial recruitment of MyD88-IRAK2 to mitochondria.

OPA1, an inner membrane dynamin-related protein, maintains the cristae junctions closed to ensure super-complex stability and assembly[45, 46, 48]. PHB forms multimeric ring complexes in the inner mitochondrial membrane, acting as a critical regulator of respiratory super-complex formation by interacting with OPA1[49]. IRAK2 was modified in IL-1R-activated adipocytes and induced to interact with PHB and OPA1 in mitochondria. We proposed that upon IL-1R activation IRAK2 is translocated into mitochondrial intermembrane space and localized on the inner membrane where it interacts with PHB, allowing PHB to recruit OPA1 away from the cristae junctions, thereby destabilizing the respiratory super-complexes. In support of this hypothesis, we found that PHB knockdown abolished the interaction of IRAK2 with OPA1 and diminished the impact of IRAK2 on super-complex formation. Interestingly, IRAK2 kinase-inactive mutant was still translocated into the mitochondria, suggesting that IRAK2 kinase activity is not required for IRAK2 interaction with TOM20 and subsequent translocation. However, the mitochondrial kinase-inactive IRAK2 lost the ability to interact with PHB-OPA1, which was accompanied by the loss of IL-1β-induced IRAK2 modification. These results suggest that IRAK2 autophosphorylation likely plays a critical role in the interaction with PHB and OPA1 in mitochondria.

We previously reported that myeloid-specific MyD88 deficiency substantially reduced diet-induced systemic inflammation and insulin resistance by preventing macrophage recruitment to adipose tissue and their switch to an M1-like phenotype[25]. We now found that adipocyte-specific MyD88 deficiency reduced diet-induced weight gain, increased whole body energy expenditure and ameliorated insulin resistance. Supported by previous studies, our findings here indicate that adipocytes in adipose tissue are not simply a passive fat storing depot, but rather constituents of a dynamic endocrine organ contributing to metabolic homeostasis[8]. We show that IL-1β was able to reprogram cell metabolism in adipocytes by driving direct IRAK2-dependent signaling in mitochondria. Importantly, while IRAK2 is required for IL-1β-induced mitochondrial function in adipocytes, it had no impact on IL-1β-induced inflammatory response in adipocytes. Thus, specifically targeting the IL-1R-IRAK2-axis in adipocytes is an especially promising approach to prevent and treat obesity, which could spare the immune system to maintain normal host defense. The future goal is to develop tailored therapeutic agents (e.g. decoy peptides) that specifically disrupt the direct interactions the IRAK2 protein with their metabolic partners, thus resetting/correcting pathogenic metabolism in adipocytes and regressing the obesity-associated pathologies.

Methods

Animals and animal care.

IRAK2-deficient and IRAK2 kinase-inactive gene-targeted mice were previously described[23, 24]. *Myd88*$^{fl/fl}$ (008888), IL-1R1-deficient (003245), Adiponectin-Cre (028020), and Ucp1-luc2, Ucp-tdTomato (026690)[50] mice were purchased from The Jackson Laboratory. HA-tagged IRAK2 reporter mice were generated by inserting 3xHA expressing cascade upstream the stop codon of *Irak2* gene (Cyagen Biosciences). HA-tagged MyD88 reporter mice were generated by inserting 3xHA expressing cascade upstream the stop

codon of *Myd88* gene (Cyagen Biosciences). IRAK2 conditionally deficient mice by flanking exon 1 of Irak2 by *lox*P sites (Cyagen Biosciences). 8-week old male mice were maintained on a high-fat diet composed of 60% kcal derived from fat (TD 06414, Envigo) for 12 weeks, while non high-fat diet mice maintained on either standard rodent chow (2918 Teklad Global 18% Protein Rodent Diet, Envigo). 6-weeks old mice were used to isolate adipose tissues for primary adipocyte culture. Animals were housed in a specific pathogen-free facility with a 14-h light/10-h dark cycle and given free access to food and water. All procedures using animals were approved by the Cleveland Clinic Institutional Animal Care and Use Committee (Protocol Number: 2018–1814).

Human samples.

Patients were recruited by the Ottawa Hospital Weight Management Clinic, Canada. The study was approved by the Ottawa Hospital IRB (Mitochondrial Function in Human Skeletal Muscle OHSN-REB, Protocol number: 2006538–01H). Omental samples were collected in weight stable patients at the time of bariatric surgery. Samples were flash frozen in liquid nitrogen and kept in −80 °C. Written informed consent was obtained from all participants.

Primary Adipocyte Culture.

Subcutaneous adipose tissues were collected from 4 to 8 weeks old mice. The tissues were minced into small pieces, followed with incubation with 3.5 mg/ml Collagenase D (Roche) in PBS buffer for 60 minutes in a 37 °C shaker water bath. The stromal vascular fraction pellet was collected after 15 min centrifugation at 280 g and filtered through 100 μm cell strainer. The cells were cultured in DMEM-F12 medium (10% PBS with 100 IU/ml Penicillin and 100 μg/ml Streptomycin) until got confluent, then differentiated in DMEM-F12 medium containing (10% PBS with 100 IU/ml penicillin and 100 μg/ml Streptomycin, 1 μM dexamethasone, 1mM IBMX, 10 μg/ml insulin) for 3 days. The cells were rested in DMEM-F12 medium (10% PBS with 100 IU/ml penicillin and 100 μg/ml Streptomycin, 10 μg/ml insulin) for 24 h before following experiment.

Mitochondria Isolation and Blue Native Polyacrylamide Gel Electrophoresis (BN-PAGE).

Mitochondrial isolation was performed according to an established protocol[51]. Differentiated primary adipocytes or 150 mg of iWAT or BAT specimen were homogenized in 2 mL ice cold isolation buffer using a Teflon Potter Elvehjem homogenizer. After homogenization, the specimen was centrifugated at 500 g for 10 min, the mitochondrial fractions were further washed and pelleted at 7000 g for 10 min for 3 times. The mitochondrial pellets were lysed in mitochondrial lysis buffer (50 mM BisTris, pH 6, 50 mM NaCl, 10% w/v Glycerol, 2% digitonin and protease inhibitors) following two rounds of centrifugation at 20,000 g for 30 min, and the clear supernatants were collected for BN-PAGE. Proteins were quantified using BCA assay (ThermoFisher). 20 mg of mitochondrial lysates with G250 Coomassie were loaded into 3%−12% NativePAGE™ Novex® Bis-Tris Gels (Invitrogen) in a Sure-Lock Xcell tank (Invitrogen), run and transferred onto PVDF membrane at 4 °C. After transfer, the membrane was rinsed with 8% acetic acid for 15 min and air-dried. Membranes were blocked with 5% milk prepared in TBST and incubated overnight at 4 °C with antibodies.

Real-time analysis of oxygen consumption rate.

The oxygen consumption rate (OCR) and extracellular acidification rate (ECAR) were measured using the Seahorse Extracellular Flux (XF24) Analyzer (Seahorse Bioscience). Newly differentiated primary adipocytes were seeded 1.5–2 × 10^4 cells per Seahorse plate well, with 4 wells per plate left empty for background correction. After indicated duration of IL-1β (10 ng/ml) or PBS stimulation, cells were washed with Seahorse assay media (supplemented with 6 mM glucose, 2 mM L-glutamine, 1 mM sodium pyruvate and the pH adjusted to 7.35 with sodium hydroxide) and the assay medium were added to bring the final volume per well to 500 μl. Three consecutive measurements were obtained under basal conditions and after the sequential addition of 1.5 μM oligomycin, to inhibit mitochondrial ATP synthase; 4.5 μM FCCP (fluoro-carbonyl cyanide phenylhydrazone), a protonophore that uncouples ATP synthesis from oxygen consumption by the electron-transport chain; and 1 μM rotenone plus 1 μM antimycin A, which inhibit the electron transport chain. In this assay, basal oxygen consumption can be established by measurement of OCR in the absence of drugs. Maximal OCR occurs after the addition of FCCP, since cells attempt to maintain a proton gradient across the inner mitochondrial membrane by increasing the consumption of oxygen by the electron-transport chain. All OCR measures were done 3 times in a 3-2-3-minute mix-wait-measure cycle.

Transmission electron microscopy and immunogold electron microscopy.

For ultrastructural analysis, cells were fixed for 1 h at 22 °C in 2% paraformaldehyde, 2.5% glutaraldehyde (Polysciences) and 0.05% malachite green (Sigma) in 100 mM sodium cacodylate buffer, pH 7.2. The malachite green was incorporated into the fixative for stabilization of lipid constituents soluble in aqueous glutaraldehyde. Samples were washed in cacodylate buffer and were post-fixed for 1 h in 1% osmium tetroxide (Polysciences). Samples were then rinsed extensively in distilled water before en bloc staining for 1 h with 1% aqueous uranyl acetate (Ted Pella). Following several rinses in distilled water, samples were dehydrated in a graded series of ethanol and embedded in Eponate 12 resin (Ted Pella). Sections 95 nm in thickness were cut with a Leica Ultracut UC7 ultramicrotome (Leica Microsystems), then were stained with uranyl acetate and lead citrate and viewed on a Tecnai G2 Spirit BioTWIN Transmission Electron Microscope (FEI Co.) at 60 kV.

For immunogold electron microscopy, samples were fixed in 0.05% glutaraldehyde and 4% paraformaldehyde PBS solution, dehydrated in increasing concentrations of ethanol up to 100%, embedded in LR white resin, and polymerized at 50 °C for 4 days. Ultrathin sections cut with a diamond knife (85 nm) were mounted on nickel grids coated with formvar. The grids were rehydrated with PBS and incubated in PBS with 0.1% BSA to block nonspecific reactions for 15 min. The sections were incubated with mouse anti-HA monoclonal antibody (Clone: HA-7, Sigma) or anti-rabbit IgG polyclonal antibody (Santa Cruz Biotechnology) at 1:50 dilution in PBS with 0.1% BSA for 3 h, washed with PBS, and then incubated for 1 h with secondary antibodies (5 nm gold-conjugated goat anti-mouse IgG from Ted Pella Inc.) at 1:10 dilution in PBS with 0.1% BSA. After PBS wash, samples were fixed with 1% glutaraldehyde in PBS for 7 min, stained briefly with uranyl acetate and lead citrate, washed with distilled water, and examined with a Tecnai G2 Spirit BioTWIN Transmission Electron Microscope (FEI Co.) at 60 kV.

Immunochemistry/immunofluorescent.

For immunohistochemistry, paraffin-embedded formalin-fixed iWAT depots were sectioned at 5 μm. After antigen retrival with sodium citrate buffer (pH 6.0) and blocking with 3% BSA in PBS solution, mouse anti-Mac2 monoclonal antibody (dil 1:50) were incubated at 4 °C overnight. The antibody was visualized using rat anti-mouse HRP-conjugated secondary antibody and the DAB substrate detection kit (BD Pharmingen). The slides were counterstained with hematoxylin and mounted, imaged with light microscope (KEYENCE). For immunofluorescent staining, frozen sections of iWAT and BAT were cut at 15 μm and blocked in 3% BSA solution (in PBS), mouse anti-RFP antibody (600-401-379, Rockland Immunochemicals, 1:200) were incubated at 4 °C overnight. After thorough rinse, the specimen was incubated with goat anti-mouse Alexa Fluor Plus 594 secondary antibody (A32744, Thermo Fisher, dil 1:500) at 22 °C for 1 h. The slides were mounted with DAPI (ThermoFisher) and imaged with confocal microscopy (KEYENCE).

Fatty acid oxidation assay.

Approximately 50 mg samples of freshly-harvested inguinal adipose tissue was harvested into tubes on ice containing a modified sucrose-EDTA buffer (250 mM sucrose, 1 mM EDTA, 10 mM Tris-HCl, 1 mM ATP, pH 7.4). After homogenization, the specimen was centrifugated at 500 g for 10 min, the mitochondrial fractions were further washed and pelleted at 7000 g for 10 min for 3 times. Resuspended mitochondria were kept on ice for immediate assay of fatty acid oxidation. Fatty acid oxidation rate was determined based on the oxidation of 1−^{14}C palmitate (Perkin-Elmer), as previously described[52]. Complete oxidation was measured by production of $^{14}CO_2$ and incomplete oxidation by production of ^{14}C -labeled acid-soluble metabolites. Total fatty acid oxidation was determined by the sum of complete and incomplete oxidation. Homogenate protein content was measured using a Bicinchoninic acid assay (ThermoFisher).

Co-immunoprecipitation and Immuno-blot analysis.

Cell were harvested and lysed on ice in a lysis buffer containing 0.5% Triton X-100, 20 mM HEPES pH 7.4,150 mM NaCl, 12.5 mM -glycerophosphate, 1.5 mM $MgCl_2$, 10 mM NaF, 2 mM dithiothreitol, 1 mM sodium orthovanadate, 2 mM EGTA, 20 mM aprotinin, and 1 mM phenylmethylsulfonyl fluoride for 20 min, followed by centrifuging at 12,000 rpm for 15 min to extract clear lysates. For immunoprecipitation, cell lysates were incubated with 1 μg of antibody and A-sepharose beads at 4 °C overnight. After incubation, the beads were washed four times with lysis buffer and the precipitates were eluted with 2x sample buffer. Elutes and whole cell extracts were resolved on SDS-PAGE followed by immune-bloting with indicated antibodies: IRAK2, Abcam, ab62419; OxPhos antibody cocktail, Abcam, ab110413; NDUFA9, Abcam, ab14713; SDHA, Abcam ab14715; Ubiquinol-Cytochrome C Reductase Core Protein I , Abcam, ab110252; MTCO1, Abcam, ab14705; ATP5A, Abcam, ab14748; VDAC, Abcam, ab154856; Cytochrome C, Abcam, ab110325; PHBa, Cell Signaling, 2426; MyD88, Cell Signaling, 4283; IRAK1, Cell Signaling, 4504; FLAG-tag, Cell Signaling, 14793; SOD2, Cell Signaling, 13194; HA-tag, Cell Signaling, 3724; β-Actin, Cell Signaling, 3700; OPA1, BD Bioscience; PHB2, ThermoFisher, PA5–14133; TOM20, Santa Cruz, sc-17764; TIMM50, Santa Cruz, sc-393678; HSP60, Cell Signaling, 4870;

Smac/Diablo, Cell Signaling, 2954; Mouse IgG, Jackson ImmunoResearch, 115-035-003; Rabbit IgG, Jackson ImmunoResearch, 111-035-144; Mouse IgG (light chain specific), Jackson ImmunoResearch, 115-035-174; Rabbit IgG (light chain specific), Jackson ImmunoResearch, 211-032-171; Rabbit IgG (Conformation Specific), Cell Signaling, 5127s.

siRNA-mediated knockdown.

siRNA-mediated knockdown: siGENOME SMARTpool siRNAs were purchased from Dharmacon (Horizon) for *Phb* knock down in adipocytes. A mixture of 4 siRNAs was used. The targeted sequences are listed below: 5'-GCGGCAACAUUUGGGCUUA-3', 5'-GUUCACAGAGGCAGUAGAA-3', 5'-GUCAAUAUCACACUGCGAA-3', 5-'GAAAGUUCGGCCUGGCGUU-3'. Non-targeting siRNA was used for the control groups with the sequence listed below: 5'-UAAGGCUAUGAAGAGAUAC-3'. Amaxa Cell Line Nucleofector Kit V (LONZA) was used to transfect adipocytes following manufacturer's instructions.

Real-time PCR.

Total RNA was extracted with TRIzol (Invitrogen) and further purified with RNeasy Lipid Tissue Mini Kit (Qiagen) according to the manufacturer's instructions. 1 μg total RNA for each sample was reverse-transcribed using the SuperScript® II Reverse Transcriptase from Thermo Fisher Scientific. The resulting complementary DNA was analyzed by real-time PCR using SYBR Green Real-Time PCR Master Mix.

Indirect calorimetry Analysis and EchoMRI.

Mice were fed a high fat diet for 12 weeks prior to study, and allowed to equilibrate to metabolic cage environments for ~48 h before entering into 24-h periods at thermoneutrality (30 °C), room temperature (22 °C), or cold temperature (4 °C). Oxygen consumption (VO_2), Carbon dioxide production (VCO_2), heat production, and respiratory exchange ratio (RER) were constantly monitored using the Oxymax CLAMS home cage system (Columbus Instruments). The data were normalized to total body weight. Fat mass and lean mass was measured by EchoMRI™−100H system (EchoMRI).

Glucose tolerance test (GTT), insulin tolerance test (ITT) and body temperature measurement.

For GTT, mice were fasted overnight and glucose (2.5 g/kg body weight) were injected peritoneally. For ITT, mice were fasted for 6 h and insulin (0.75 U/kg body weight) were injected peritoneally. Blood glucose level was measured by AimStrip Plus Blood Glucose Testing System (Germaine Laboratories). Rectal temperature was measured by MicroTherma 2T Hand Held Thermometer with a rectal probe (Braintree Scientific).

Mitochondrial DNA Release Assay.

DNA was isolated from 200 μl of the cytosolic fraction using a DNeasy Blood & Tissue Kit (Qiagen) according to manufacturer's instruction. Quantitative PCR was employed to measure mtDNA using real-time PCR using SYBR Green Real-Time PCR Master Mix. The copy number of mtDNA encoding cytochrome c oxidase I was normalized to nuclear DNA

encoding 18S ribosomal DNA. The following primers were used: cytochrome c oxidase I *mt-Co1* (F: 5'- GCCCCAGATATAGCATTCCC-3' and R: 5'-GTTCATCCTGTTCCTGCTCC-3') and 18S rDNA *Rn18s* (F: 5'-TAGAGGGACAAGTGGCGTTC-3' and R: 5'-CGCTG AGCCAGTCAGTGT-3').

Spectrophotometric assays of mitochondrial respiratory complex activity.

The activities of mitochondrial respiratory complexes were assayed spectrophotometrically using sonicated, thawed mitochondria samples at 22 °C as described previously[53, 54, 55]. Complex I (NADH-ubiquinone reductase) activity assay: The electron transfer activity of complex I was assayed by ubiquinone-stimulated NADH oxidation. 5 mg of mitochondrial protein were mixed with 100 μl assay buffer (20 mM potassium phosphate buffer, 2 mM NaN_3, 0.8% sodium cholate, 0.15 mM NADH, pH 8.0). The reaction was initiated by the addition of 0.1 mM ubiquinone-1 (CoQ1) and the change of absorbance for NADH was measured at 340 nm ($\varepsilon = 6.22\ mM^{-1}\ cm^{-1}$). The specificity of the assay was validated by rotenone-sensitive inhibition. Complex I activity was expressed as the oxidation rate of NADH (nmol NADH oxidized/min/mg protein). Complex III (ubiquinol-cytochrome c reductase) activity assay: Complex III activity was evaluated by ubiquinol-mediated ferricytochrome c reduction at 550 nm ($\varepsilon = 18.5\ mM^{-1}\ cm^{-1}$) upon addition of 1 μg protein to 100 μl assay buffer (50 mM potassium phosphate buffer, 1 mM EDTA, 50 μM cytochrome c, 0.1% sodium cholate, 2 mM NaN_3 and 25 μM ubiquinol, pH 7.0). Inhibition of the assay with Antimycin A was used to verify the specificity of assay. Complex III activity was expressed as the reduction rate of ferricytochrome c (nmol ferricytochrome c reduced/min/mg protein). Complex I + Complex III activity assay: Complex I + III activity was evaluated by NADH-ubiquinone-mediated ferricytochrome c reduction at 550 nm ($\varepsilon = 18.5\ mM^{-1}\ cm^{-1}$) upon addition of 1 μg protein to 100 μl assay buffer (25 mM potassium phosphate buffer, 2 mM NaN_3, 0.8% sodium cholate, 0.15 mM NADH, 1 mM EDTA, 50 μM cytochrome c and 0.1 mM CoQ1). Complex I + III activity was expressed as the reduction rate of ferricytochrome c (nmol ferricytochrome c reduced/min/mg protein).

Cytosolic calcium Assay.

Cytosolic fraction was isolated as described above. Calcium levels were measured using Calcium Assay Kit (Cayman Chemical) according to manufacturer's instruction.

Non-radioactive fatty acid oxidation (FAO) assay.

The non-radioactive FAO assay is based on oxidation of the substrate octanoyl-carnitine. Generation of NADH is coupled to the reduction of the tetrazolium salt INT to formazan. The intensity of the red-colored formazan (measured at 492 nm) is proportional to increased FAO activity. Fatty Acid Oxidation Assay Kit (Biomedical Research Service & Clinical Application) was used after replacing the substrate from octanoyl-CoA to octanoyl-carnitine (Cayman).

Cellular ROS and ATP Assay.

Cellular ROS and ATP levels were measured using the DCFDA Cellular ROS Detection Assay Kit (Abcam) and Luminescent ATP Detection Assay Kit (Abcam) according to manufacturer's instruction.

Mitochondrial Sub-fractionation.

Separation of inner and outer mitochondrial membranes was performed as described[56, 57, 58]. Purified adipocytes' mitochondria from 50 15-cm cell culture plates were re-suspended in hypotonic medium (10 mM KCl, 2 mM HEPES, pH 7.2) at 10 mg/ml with gentle stirring for 20 min on ice. One-third volume of hypertonic medium (1.8 mM sucrose, 2 mM ATP, 2 mM $MgSO_4$, 2 mM HEPES, pH 7.2) was then added and the solution stirred for an additional 5 min. The mitochondria were sonicated for 15 seconds at 3 amps before being layered on top of a stepwise gradient of 0.76, 1.0, 1.32, and 1.8 M sucrose and spun at 75,000 g for 3 h in an SW40 Ti rotor (Beckman). The soluble intermembrane space (IMS) fraction was collected from the upper supernatant, the outer membrane (OM) from between the 0.76 and 1.0 M interface, and the mitoplasts (MP) from the pellet. The MP and OM fractions were washed with MSHE and re-pelleted (MP at 10,000 g for 10 min, OM at 120,000 g for 45 min). MP were sonicated 3 × 2 min on ice with 1-min intervals. The solution was spun at 15,000 g to remove intact MP, and the resulting supernatant was spun at 120,000 g for 45 min at 4 °C to pellet inner membrane (IM). The soluble matrix (SM) fraction was collected from the supernatant.

Statistical analysis.

The significance of differences between two groups was determined by Student's t-test (two-tailed). All mouse data were analyzed using either one-way or two-way ANOVA, where appropriate, followed by post hoc analysis. Differences were considered significant at $p<0.05$. All data analyses were performed using ImageJ or GraphPad Prism 6 software.

Data Availability Statement.

The primary data for analysis of all figures and supplementary figures are available upon request.

Extended Data

a. Characteristics of Patients, Related to Figure 1a

Factor	Total (N=48)	Non-diabetic (N=25)	Diabetic (N=23)
Demographic			
Age	47.4 (27-64)	45.8 (27-64)	49.1 (36-60)
Male (%)	2 (4.1)	2 (4.1)	0 (0)
BMI	49.4 (37.2-67.9)	50.8 (40.6-67.9)	47.8 (37.2-64.3)
Clinical			
Cholesterol	4.6 (2.6-7.8)	4.8 (3.4-7.8)	4.4 (2.6-6.7)
Triglycerides	1.9 (0.7-9.1)	1.5 (0.7-3.6)	2.4 (0.8-9.1)
LDL	2.6 (0.9-5.5)	2.8 (0.9-5.5)	2.4 (0.9-4.5)
HDL	1.3 (0.6-3.5)	1.3 (0.6-3.5)	1.2 (0.7-2.3)
Glucose	6.2 (4.5-12.0)	5.3 (4.5-7.2)	7.2 (5.0-12.0)
Creatinine	60.5 (41-95)	61.1 (41-95)	59.9 (42-93)
hgbA1c	0.06 (0.05-0.08)	0.06 (0.05-0.07)	0.07 (0.06-0.08)

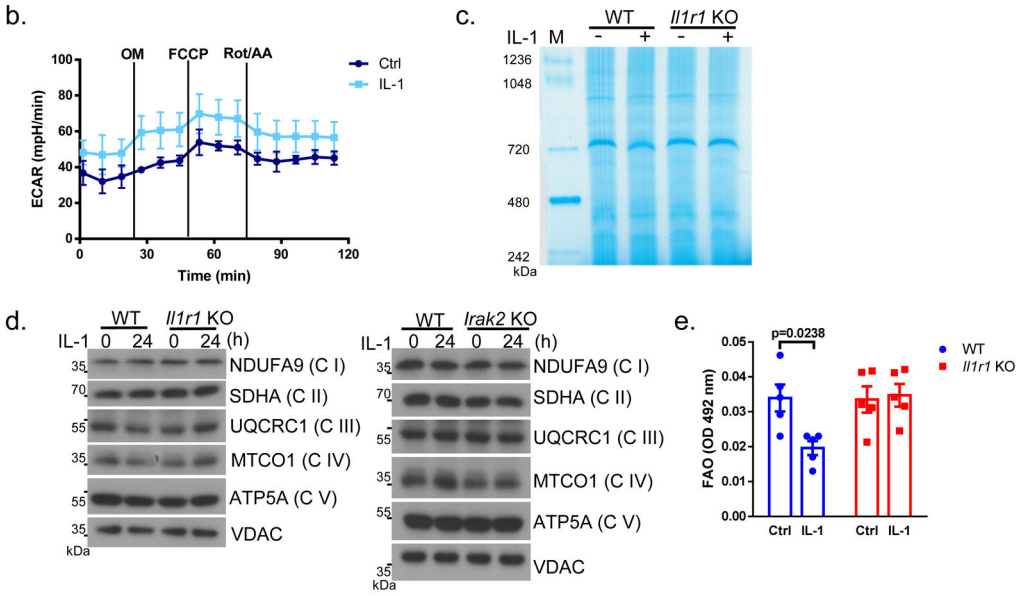

Extended Data Fig. 1. Extended information related to Fig. 1.

a. Characteristics of patients, related to Fig. 1a. **b.** Extracellular acidification rate (ECAR), related to Fig. 1d. Data represent mean ± SEM. Data represent one of five independent experiments with similar results. **c.** Coomassie blue staining of mitochondrial proteins, related to Fig. 1e. **d.** Mitochondrial proteins were extracted from WT and *Il1r1* KO; WT and *Irak2* KO newly differentiated primary adipocytes treated with or without IL-1β for indicated time points and analyzed by SDS-PAGE, followed by western blot analysis with indicated antibodies. Data represent one of five independent experiments with similar results. **e.** Octanoyl-carnitine oxidation-rate in isolated mitochondria from WT and *Il1r1* KO primary adipocytes treated with or without IL-1β (n=4). Student's t-test (two-tailed) was performed. Data represent mean ± SEM.

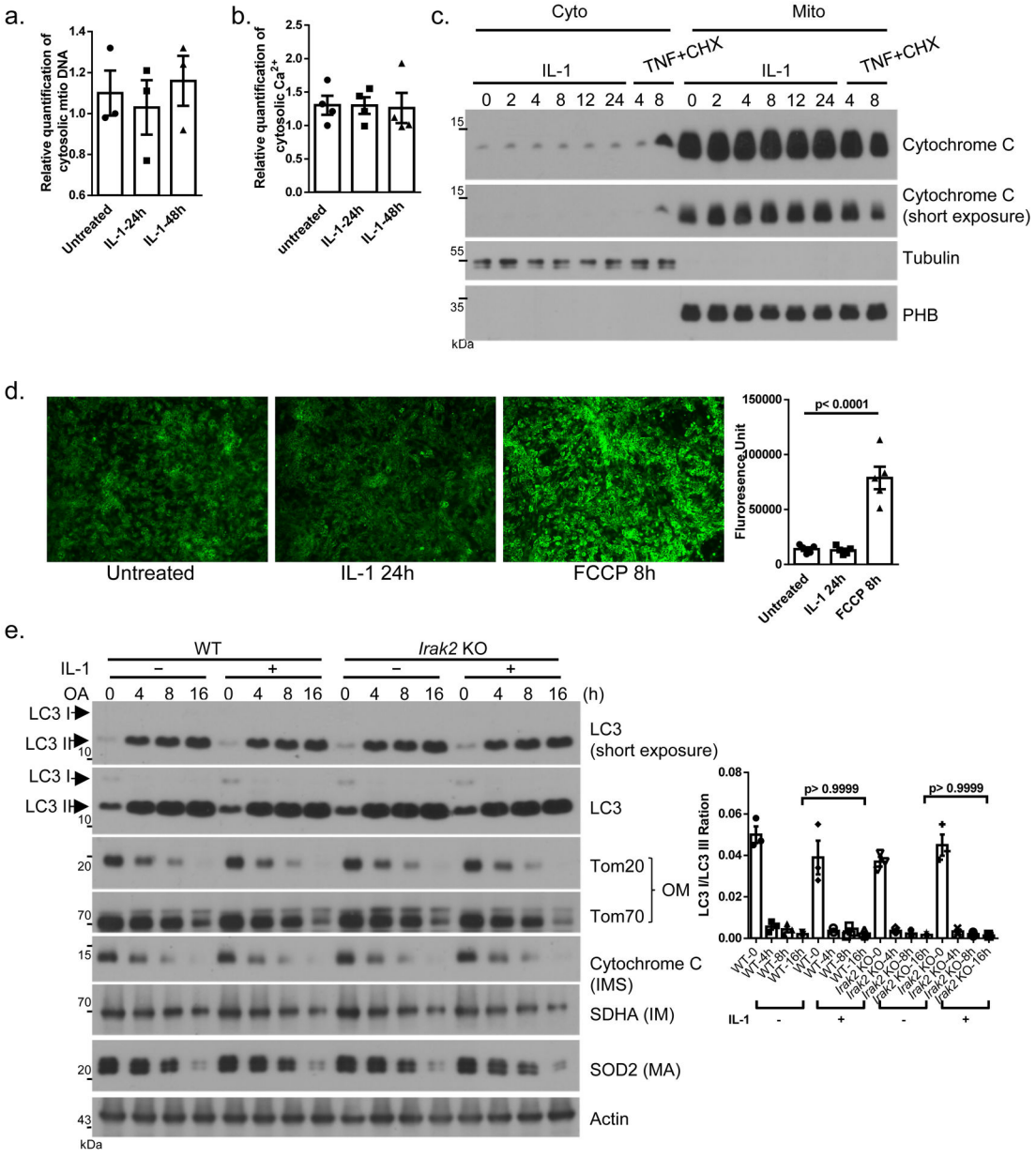

Extended Data Fig. 2. IL-1 stimulation did not lead to mitochondria dysfunction.

Newly differentiated primary adipocytes were treated with IL-1β for indicated time points. Cytosolic mtDNA (n=3) (**a**) and cytosolic Ca^{2+} (n=4) (**b**) levels were measured. **c.** Western blot analysis of cytoplasmic and mitochondrial proteins from IL-1β or TNFα + cycloheximide (CHX) treated newly differentiated primary adipocytes. Data represent one of five independent experiments with similar results. **d.** Newly differentiated primary adipocytes were treated with IL-1β or trifluoromethoxy carbonylcyanide phenylhydrazone (FCCP) for indicated time points. Cellular reactive oxygen species (ROS) were measured using fluorescent microscopy and microplate reader (n=5). **e.** Western blot analysis of cytoplasmic and mitochondrial proteins from oligomycin + antimycin (OA) treated newly differentiated WT and *Irak2* KO primary adipocytes (pretreated with IL-1β or PBS). Data

represent one of five independent experiments with similar results. Densitometric analysis of LC3 I/LC3 III were listed a bar graph (n=3). **a, b, e**: Student's t-test (two-tailed) was performed. Data represent mean ± SEM. **d**: One-way ANOVA was performed. Data represent mean ± SEM.

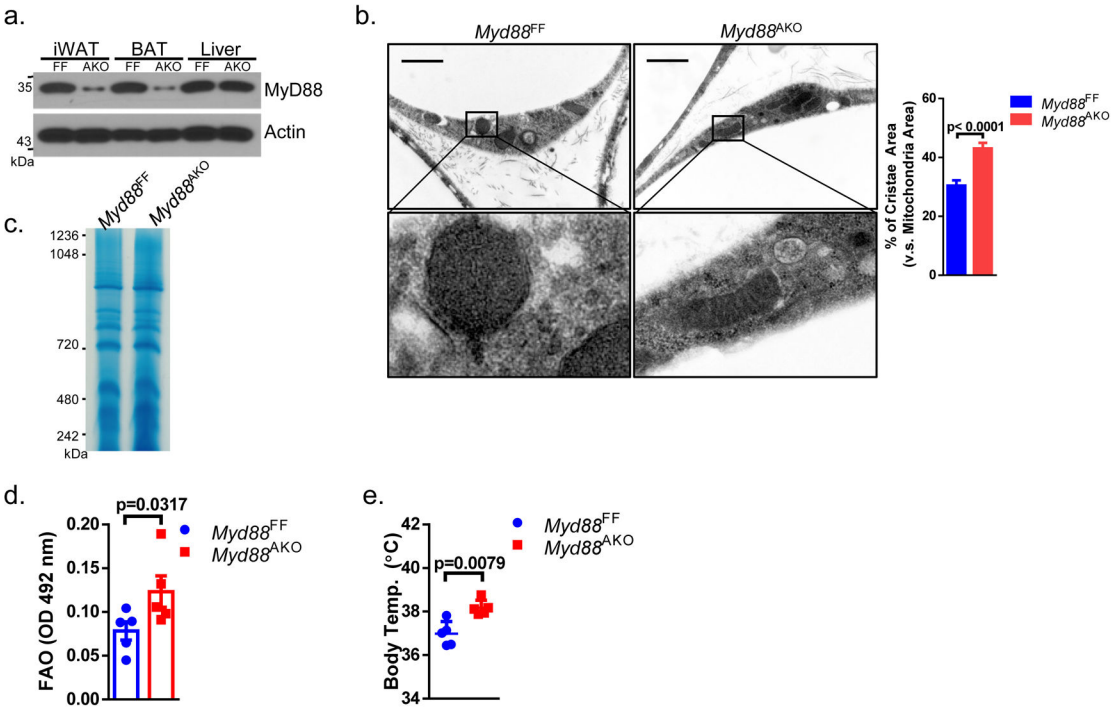

Extended Data Fig. 3. Extended information related to Fig. 2.

a. Total lysates from iWAT, BAT and liver from *Myd88*^{FF} and *Myd88*^{AKO} mice were subjected to western blot analysis with indicated antibodies. Data represent one of five independent experiments with similar results. **b.** Transmission electron microscopy analysis of iWAT sections from HFD-fed mice. Scale bars, 1 μm. Morphometric analysis of cristae area versus mitochondria area in 40 randomly selected mitochondria per group. **c.** Coomassie blue staining of mitochondrial proteins, related to Fig. 2i. **d.** Octanoyl-carnitine oxidation-rate in isolated mitochondria from BAT of HFD-fed mice with indicated genotypes (n=5). **e.** Rectal temperatures were measured for HFD-fed mice with indicated genotypes (n=5). **b, d, e:** Student's t-test (two-tailed) was performed. Data represent mean ± SEM.

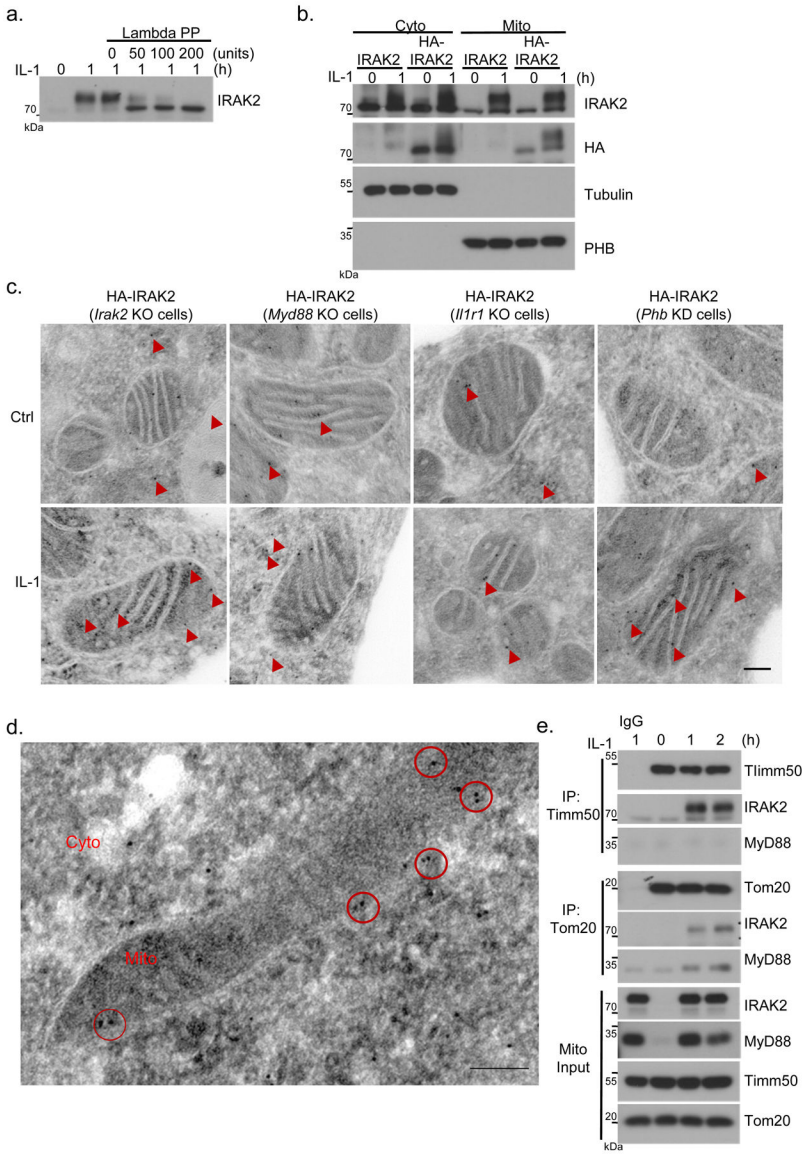

Extended Data Fig. 4. Extended information related to Fig. 3.

a. Western blot analysis of immune-precipitated IRAK2 from IL-1β treated mitochondria and subjected to indicated amount of Lambda phosphatase (Lambda PP) treatment for 10 min. **b.** Wild-type and HA-tagged IRAK2 were restored in *Irak2* KO adipocytes. Western blot analysis of cytoplasmic and mitochondrial proteins from IL-1β treated cells. **c.** Immunogold staining of HA-tagged IRAK2 which was overexpressed in *Irak2* KO, *Myd88* KO, *Il1r1* KO and *Phb* KD cells with or without IL-1 treatment for 24h. Scale bars, 50 nm. **d.** Immunogold staining of HA-tagged MyD88 in newly differentiated primary adipocytes from *Myd88*-HA reporter mice. Mito: mitochondrion; Cyto: cytosol. Scale bar, 200 nm. **e.** Co-immunoprecipitation (IP) analysis of TIMM50 and TOM20 in mitochondria of in newly differentiated primary adipocytes from IRAK2-HA reporter mice treated with IL-1β for indicated time points and followed by western blot analysis. **a, b, e**: Data represent one of five independent experiments with similar results.

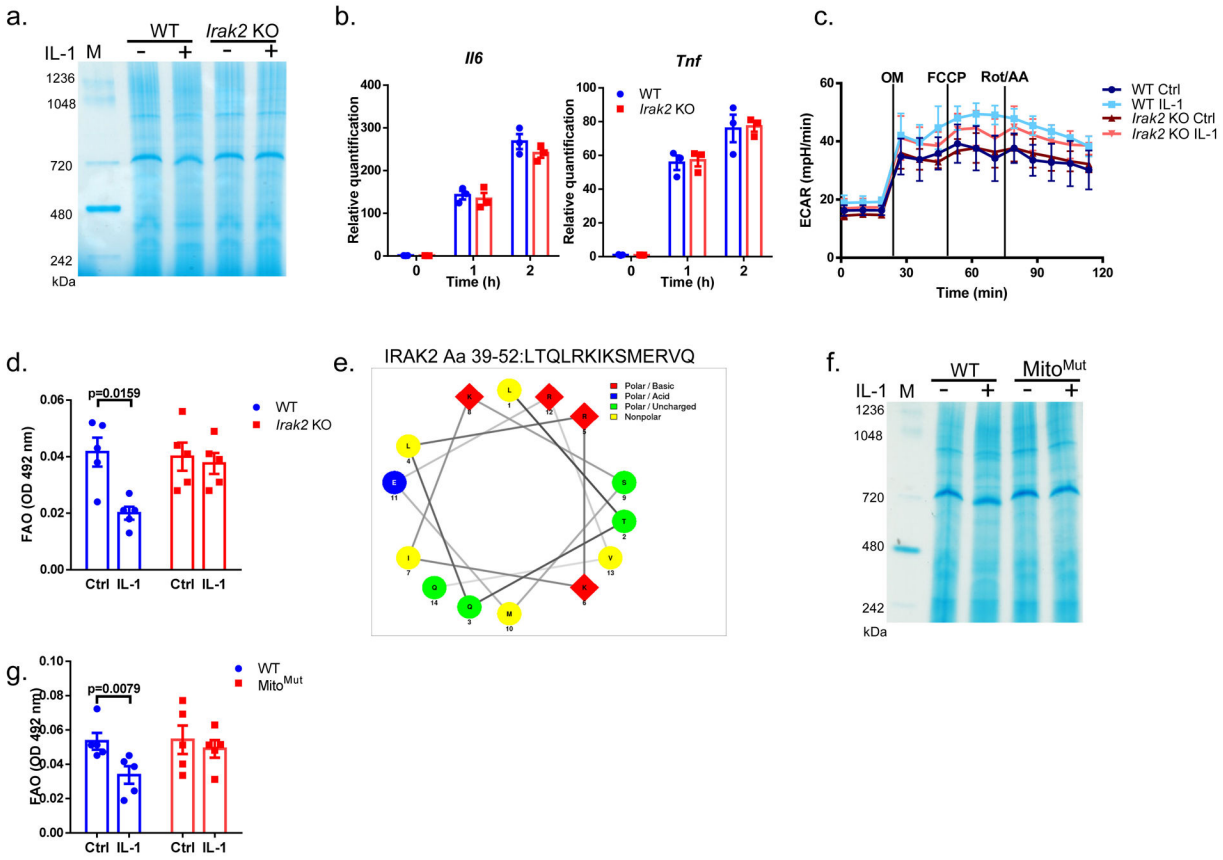

Extended Data Fig. 5. Extended information related to Fig. 3.

a. Coomassie blue staining of mitochondrial proteins, related to Fig. 3d. **b.** Expression of indicated mRNAs in WT and *Irak2* KO newly differentiated primary adipocytes treated with or without IL-1β for indicated time points (n=3). **c.** Extracellular acidification rate (ECAR), related to Fig. 3f. Data represent mean ± SEM. Data represent one of five independent experiments with similar results. **d.** Octanoyl-carnitine oxidation-rate in isolated mitochondria from WT and *Irak2* KO primary adipocytes treated with or without IL-1β for 24h (n=5). **e.** Secondary helical wheel structure of IRAK2 peptide (amino acid: 39–52) which contains mitochondrial localization signal (MLS). The picture was generated by http://lbqp.unb.br/NetWheels/. **f.** Coomassie blue staining of mitochondrial proteins, related to Fig. 3k. **g.** Octanoyl-carnitine oxidation-rate in isolated mitochondria from Flag-tagged wild-type and IRAK2 mito-mutant restored *Irak2* KO adipocytes treated with or without IL-1β for 24h (n=5). **b, d, g:** Student's t-test (two-tailed) was performed. Data represent mean ± SEM.

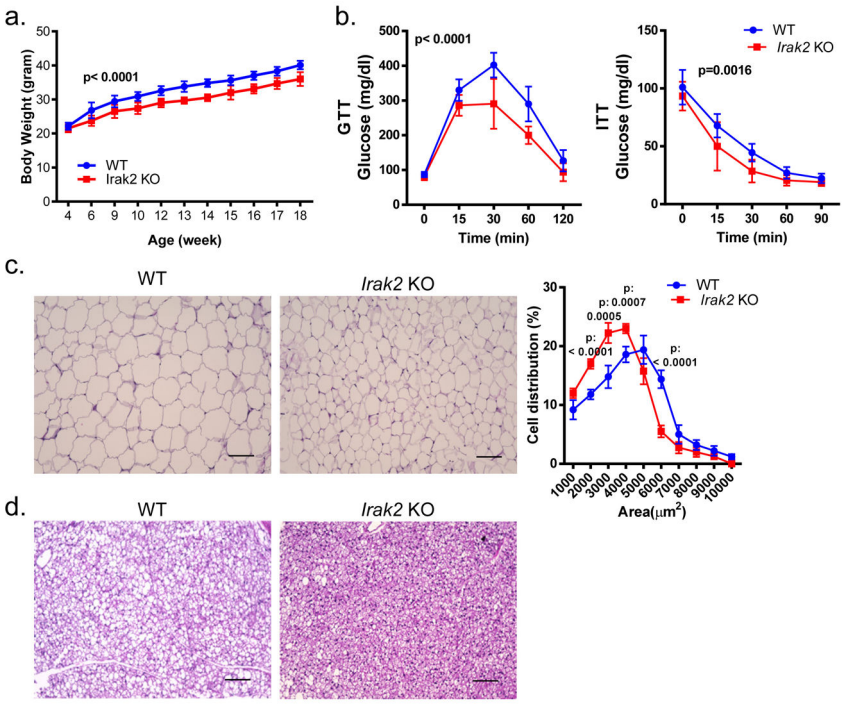

Extended Data Fig. 6. Extended information related to Fig. 4.

a. Body weight of WT and *Irak2* KO mice on HFD feeding (n=6 females per group). **b.** Glucose tolerance test (GTT) and insulin tolerance test (ITT) were performed on HFD-fed of WT and *Irak2* KO mice (n=5 females per group). **c.** H&E staining of iWAT sections from HFD-fed of WT and *Irak2* KO mice. Cell size was quantified (3 views per slide, 3 sections per mouse, n=5). **d.** H&E staining of BAT sections from HFD-fed of WT and *Irak2* KO mice. **c, d**: scale bars, 150 μm. **a, b**: Two-way ANOVA, followed by post hoc analysis was performed. Data represent mean ± SEM. **c**: Student's t-test (two-tailed) was performed. Data represent mean ± SEM.

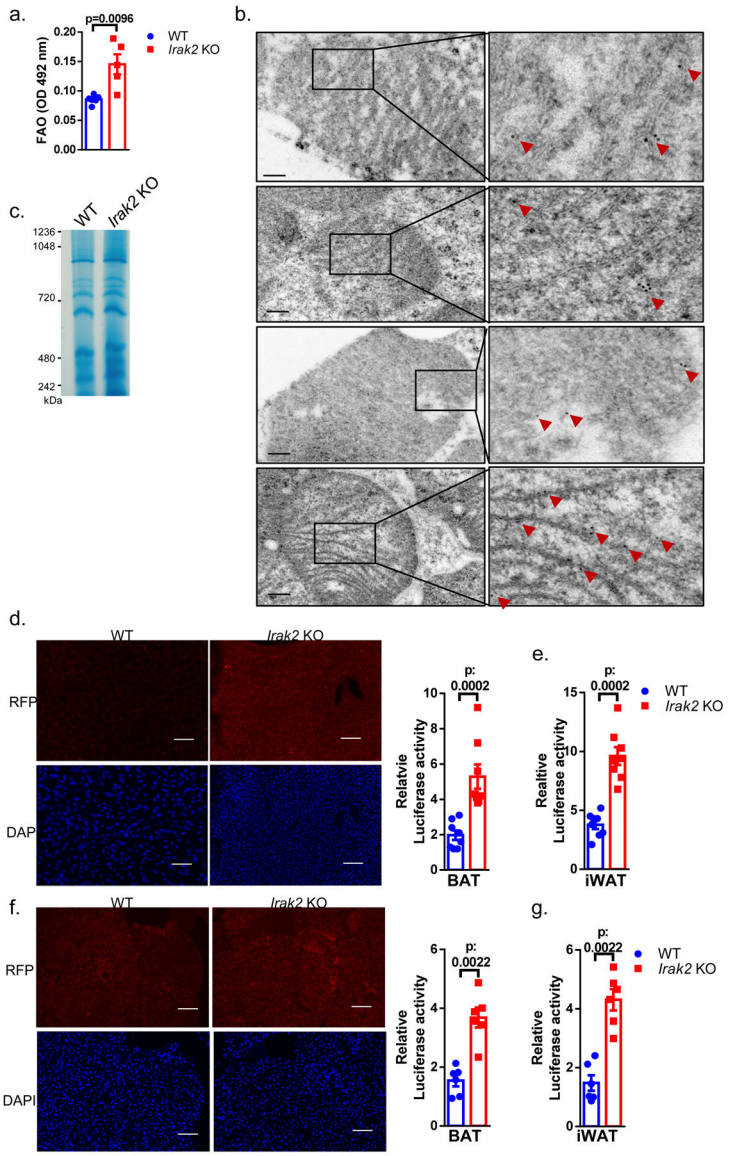

Extended Data Fig. 7. Extended information related to Fig. 5.

a. Octanoyl-carnitine oxidation-rate in isolated mitochondria from BAT of HFD-fed mice with indicated genotypes (n=5). **b.** Various pictures of immunogold staining of HA-tagged IRAK2 in BAT sections of HFD-fed *Irak2*-HA reporter mice, related to Fig. 5c Scale bars, 200nm. **c.** Coomassie blue staining of mitochondrial proteins, related to Fig. 5e. **d-e.** Immunohistochemical staining of RFP in BAT sections of HFD-fed WT and *Irak2* KO Ucp1-luc/tdTomato reporter mice. Luciferase enzymatic activity in lysates from BAT (d) and iWAT (e) (n=8). **f-g.** HFD-fed WT and *Irak2* KO Ucp1-luc/tdTomato reporter mice injected with CL-316,243 for 3 days. Immunohistochemical staining of RFP in BAT sections and Luciferase enzymatic activity in lysates from BAT (L) and iWAT (M) (n=6). **d, f**: Scale bars, 150 nm. **a, d, e, f, g:** Student's t-test (two-tailed) was performed. Data represent mean ± SEM.

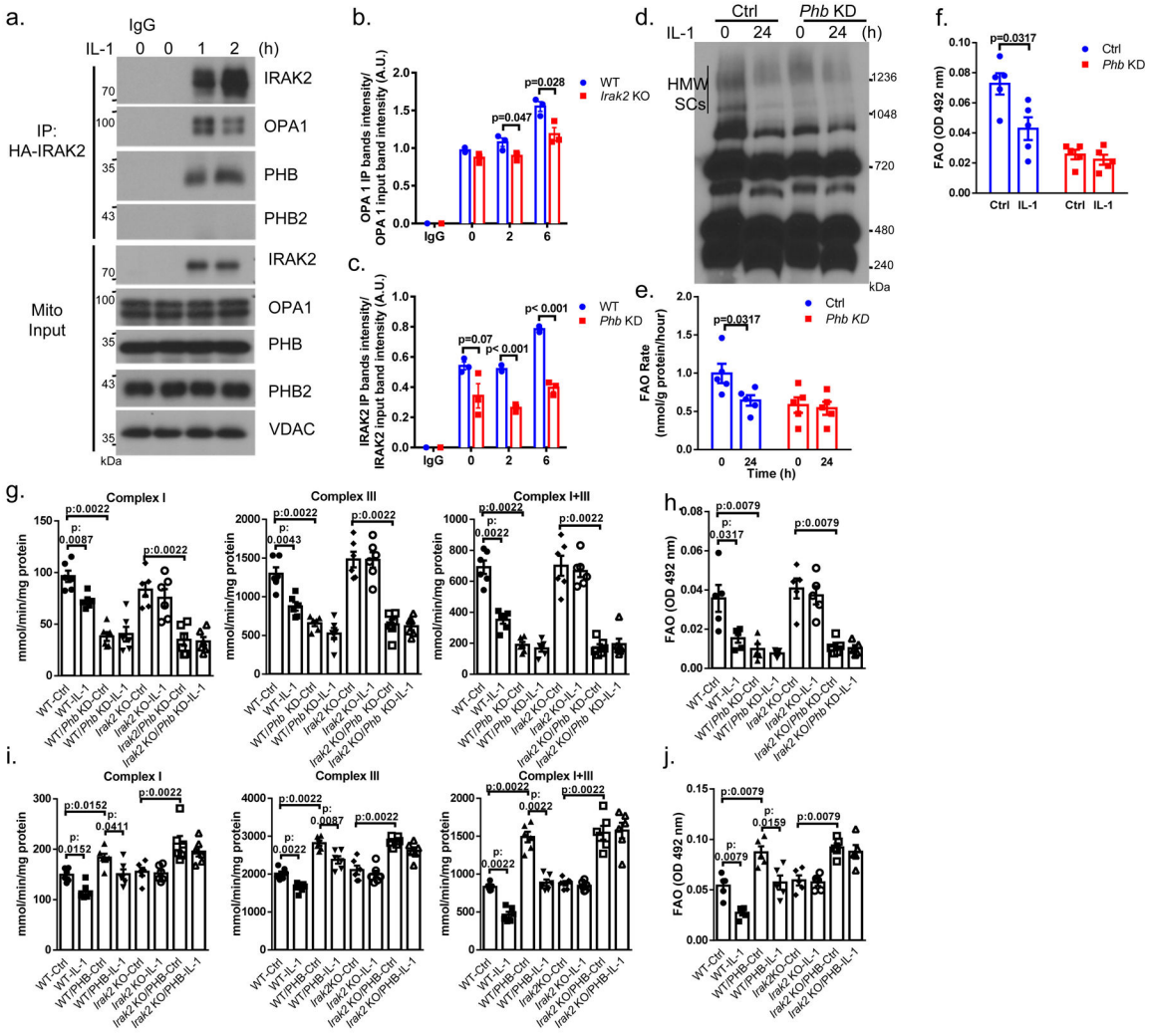

Extended Data Fig. 8. Extended information related to Fig. 6.

a. Co-immunoprecipitation (IP) analysis of HA-tagged IRAK2, in mitochondria of in newly differentiated primary adipocytes from *Irak2*-HA reporter mice treated with IL-1β for indicated time points and followed by western blot analysis. Data represent one of five independent experiments with similar results. **b, c**: Densitometric analysis of western blots in Fig. 6a and 6b. **b.** Signals corresponding to IP OPA1 were used and normalized to Mito input OPA1 in Fig. 6a (n=3). **c.** Signals corresponding to IP IRAK2 were used and normalized to Mito input IRAK2 in Fig. 6b (n=3). **d,** Mitochondrial proteins were extracted Ctrl and *Phb* KD primary adipocytes treated with IL-1β for indicated time points and analyzed by BN-PAGE, followed by Western blot analysis with anti-OxPhos cocktail antibodies. HMW SCs: high molecular weight super-complexes. **e.** [1-^{14}C]-palmitic acid oxidation-rate **f.** Octanoyl-carnitine oxidation-rate in isolated mitochondria from WT and *Phb* KD primary adipocytes, treated with or without IL-1β for 24h (n=5). **g.** The activities of respiratory complexes **h.** Octanoyl-carnitine oxidation-rate in the isolated mitochondria in mitochondria of non-targeting siRNA (WT and *Irak2* KO) and PHB siRNA transfected (WT/ *Phb* KD, *Irak2* / *Phb* KD) WT and *Irak2* KO primary adipocytes treated with/without IL-1β

(n=6). **i.** The activities of respiratory complexes **j.** Octanoyl-carnitine oxidation-rate in the isolated mitochondria in mitochondria of empty vector (WT and *Irak2* KO) and PHB cDNA transfected (WT/PHB and *Irak2* KO/PHB) WT and *Irak2* KO primary adipocytes treated with/without IL-1β (n=6). **b, c, e, f, g, h, i, j**: Student's t-test (two-tailed) was performed. Data represent mean ± SEM.

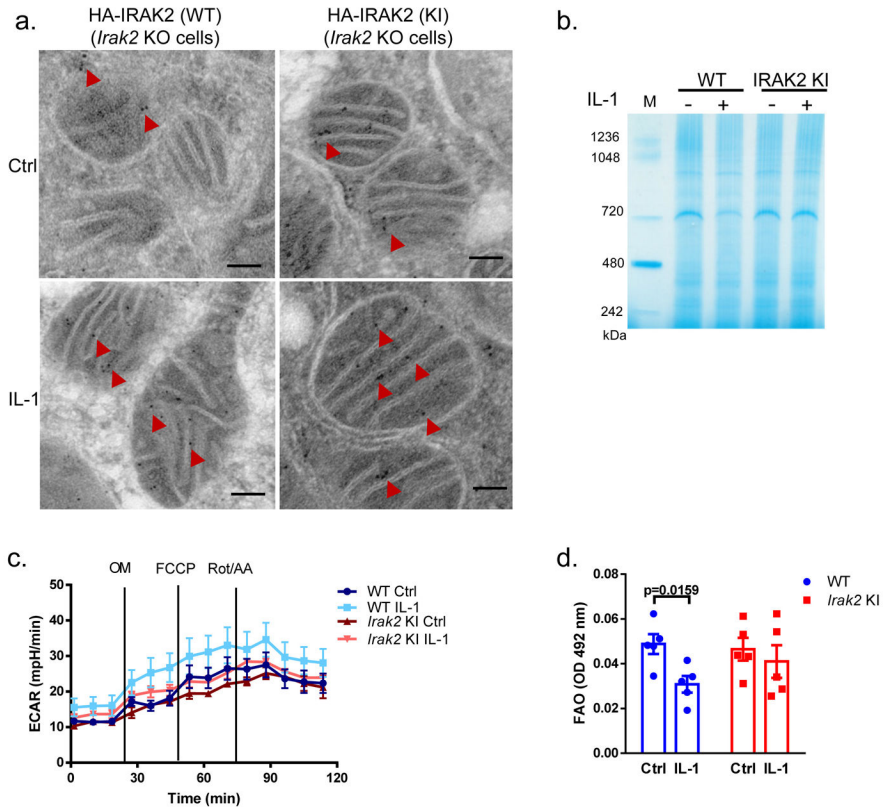

Extended Data Fig. 9. Extended information related to Fig. 6.

a. Immunogold staining of HA-tagged IRAK2 and kinase-inactive (KI) mutant which were overexpressed in *Irak2* KO cells with or without IL-1β treatment for 24h. Scale bars, 50 nm. **b.** Coomassie blue staining of mitochondrial proteins, related to Fig. 6d. **c.** Extracellular acidification rate (ECAR), related to Fig. 6g. Data represent mean ± SEM. Data represent one of five independent experiments with similar results. **d.** Octanoyl-carnitine oxidation-rate in isolated mitochondria from WT and *Irak2* KI primary adipocytes, treated with or without IL-1β for 24h (n=5). Student's t-test (two-tailed) was performed. Data represent mean ± SEM.

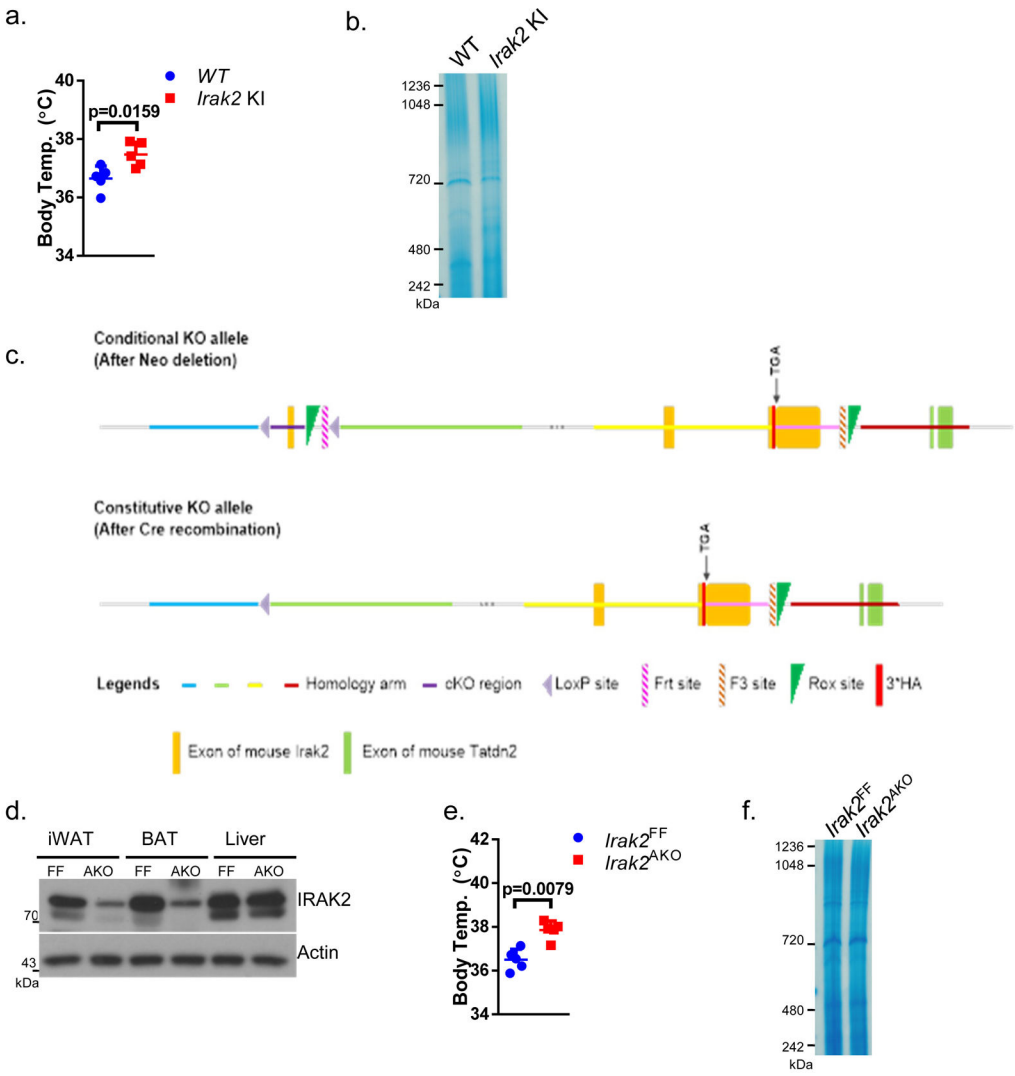

Extended Data Fig. 10. Extended information related to Fig. 7 & 8.

a. Rectal temperatures were measured for HFD-fed mice with indicated genotypes (n=5) **b.** Coomassie blue staining of mitochondrial proteins, related to Fig. 7g. **c.** Targeting vector design for generation of a novel mouse strain with exon 1 of Irak2 flanked by *lox*P sites. **d.** Total lysates from iWAT, BAT and liver from *Irak2*^{FF} and *Irak2*^{AKO} mice were subjected to western blot analysis with indicated antibodies. Data represent one of five independent experiments with similar results. **e.** Rectal temperatures were measured for HFD-fed mice with indicated genotypes (n=5). f. Coomassie blue staining of mitochondrial proteins, related to Fig. 8g. **a, c:** Student's t-test (two-tailed) was performed. Data represent mean ± SEM.

Supplementary Material

Refer to Web version on PubMed Central for supplementary material.

Acknowledgment

This work was supported by grants from NIH (2P01HL029582, R01AA023722, P01CA062220, R01HL122283, and P50AA024333) and National MS society (RG5130A2/1). H.Z was supported by Postdoctoral Research Fellow Award (1-16-PDF-138) from American Diabetes Association.

References

1. Bozkurt B et al. Contributory Risk and Management of Comorbidities of Hypertension, Obesity, Diabetes Mellitus, Hyperlipidemia, and Metabolic Syndrome in Chronic Heart Failure: A Scientific Statement From the American Heart Association. Circulation 134, e535–e578 (2016). [PubMed: 27799274]
2. Grundy SM Metabolic syndrome update. Trends Cardiovasc Med 26, 364–373 (2016). [PubMed: 26654259]
3. Said S, Mukherjee D & Whayne TF Interrelationships with Metabolic Syndrome, Obesity and Cardiovascular Risk. Curr Vasc Pharmacol 14, 415–425 (2016). [PubMed: 27456105]
4. Juge-Aubry CE et al. Adipose tissue is a major source of interleukin-1 receptor antagonist: upregulation in obesity and inflammation. Diabetes 52, 1104–1110 (2003). [PubMed: 12716739]
5. Greenberg AS & Obin MS Obesity and the role of adipose tissue in inflammation and metabolism. Am J Clin Nutr 83, 461S–465S (2006). [PubMed: 16470013]
6. Weisberg SP et al. Obesity is associated with macrophage accumulation in adipose tissue. J Clin Invest 112, 1796–1808 (2003). [PubMed: 14679176]
7. Sun K, Kusminski CM & Scherer PE Adipose tissue remodeling and obesity. J Clin Invest 121, 2094–2101 (2011). [PubMed: 21633177]
8. Kershaw EE & Flier JS Adipose tissue as an endocrine organ. J Clin Endocrinol Metab 89, 2548–2556 (2004). [PubMed: 15181022]
9. Ballak DB, Stienstra R, Tack CJ, Dinarello CA & van Diepen JA IL-1 family members in the pathogenesis and treatment of metabolic disease: Focus on adipose tissue inflammation and insulin resistance. Cytokine 75, 280–290 (2015). [PubMed: 26194067]
10. Cortez M, Carmo LS, Rogero MM, Borelli P & Fock RA A high-fat diet increases IL-1, IL-6, and TNF-alpha production by increasing NF-kappaB and attenuating PPAR-gamma expression in bone marrow mesenchymal stem cells. Inflammation 36, 379–386 (2013). [PubMed: 23079940]
11. Nov O et al. Interleukin-1beta regulates fat-liver crosstalk in obesity by auto-paracrine modulation of adipose tissue inflammation and expandability. PLoS One 8, e53626 (2013). [PubMed: 23341960]
12. Serena C et al. Obesity and Type 2 Diabetes Alters the Immune Properties of Human Adipose Derived Stem Cells. Stem Cells 34, 2559–2573 (2016). [PubMed: 27352919]
13. Krautbauer S et al. Free fatty acids, lipopolysaccharide and IL-1alpha induce adipocyte manganese superoxide dismutase which is increased in visceral adipose tissues of obese rodents. PLoS One 9, e86866 (2014). [PubMed: 24475187]
14. Schaeffler A et al. Fatty acid-induced induction of Toll-like receptor-4/nuclear factor-kappaB pathway in adipocytes links nutritional signalling with innate immunity. Immunology 126, 233–245 (2009). [PubMed: 18624726]
15. Garcia MC et al. Mature-onset obesity in interleukin-1 receptor I knockout mice. Diabetes 55, 1205–1213 (2006). [PubMed: 16644674]
16. Dascombe MJ, Hardwick A, Lefeuvre RA & Rothwell NJ Impaired effects of interleukin-1 beta on fever and thermogenesis in genetically obese rats. Int J Obes 13, 367–373 (1989). [PubMed: 2788629]
17. del Rey A, Monge-Arditi G, Klusman I & Besedovsky HO Metabolic and endocrine effects of interleukin-1 in obese, diabetic Zucker fa/fa rats. Exp Clin Endocrinol Diabetes 104, 317–326 (1996). [PubMed: 8886749]
18. Matsuki T, Horai R, Sudo K & Iwakura Y IL-1 plays an important role in lipid metabolism by regulating insulin levels under physiological conditions. J Exp Med 198, 877–888 (2003). [PubMed: 12975454]

19. Somm E et al. Decreased fat mass in interleukin-1 receptor antagonist-deficient mice: impact on adipogenesis, food intake, and energy expenditure. Diabetes 54, 3503–3509 (2005). [PubMed: 16306368]
20. Kawai T & Akira S Toll-like receptors and their crosstalk with other innate receptors in infection and immunity. Immunity 34, 637–650 (2011). [PubMed: 21616434]
21. Lin SC, Lo YC & Wu H Helical assembly in the MyD88-IRAK4-IRAK2 complex in TLR/IL-1R signalling. Nature 465, 885–890 (2010). [PubMed: 20485341]
22. Yao J et al. Interleukin-1 (IL-1)-induced TAK1-dependent Versus MEKK3-dependent NFkappaB activation pathways bifurcate at IL-1 receptor-associated kinase modification. J Biol Chem 282, 6075–6089 (2007). [PubMed: 17197697]
23. Wan Y et al. Interleukin-1 receptor-associated kinase 2 is critical for lipopolysaccharide-mediated post-transcriptional control. J Biol Chem 284, 10367–10375 (2009). [PubMed: 19224918]
24. Zhou H et al. IRAK2 directs stimulus-dependent nuclear export of inflammatory mRNAs. Elife 6 (2017). DOI: 10.7554/eLife.29630
25. Yu M et al. MyD88-dependent interplay between myeloid and endothelial cells in the initiation and progression of obesity-associated inflammatory diseases. J Exp Med 211, 887–907 (2014). [PubMed: 24752299]
26. Everts B et al. TLR-driven early glycolytic reprogramming via the kinases TBK1-IKKvarepsilon supports the anabolic demands of dendritic cell activation. Nat Immunol 15, 323–332 (2014). [PubMed: 24562310]
27. Huang YL et al. Toll-like receptor agonists promote prolonged triglyceride storage in macrophages. J Biol Chem 289, 3001–3012 (2014). [PubMed: 24337578]
28. Salerno F, Guislain A, Cansever D & Wolkers MC TLR-Mediated Innate Production of IFN-gamma by CD8+ T Cells Is Independent of Glycolysis. J Immunol 196, 3695–3705 (2016). [PubMed: 27016606]
29. Tannahill GM et al. Succinate is an inflammatory signal that induces IL-1beta through HIF-1alpha. Nature 496, 238–242 (2013). [PubMed: 23535595]
30. Xu H et al. Chronic inflammation in fat plays a crucial role in the development of obesity-related insulin resistance. J Clin Invest 112, 1821–1830 (2003). [PubMed: 14679177]
31. Cani PD et al. Metabolic endotoxemia initiates obesity and insulin resistance. Diabetes 56, 1761–1772 (2007). [PubMed: 17456850]
32. Shi H et al. TLR4 links innate immunity and fatty acid-induced insulin resistance. J Clin Invest 116, 3015–3025 (2006). [PubMed: 17053832]
33. Juge-Aubry CE et al. Regulatory effects of interleukin (IL)-1, interferon-beta, and IL-4 on the production of IL-1 receptor antagonist by human adipose tissue. J Clin Endocrinol Metab 89, 2652–2658 (2004). [PubMed: 15181037]
34. Letts JA & Sazanov LA Clarifying the supercomplex: the higher-order organization of the mitochondrial electron transport chain. Nat Struct Mol Biol 24, 800–808 (2017). [PubMed: 28981073]
35. Wesche H, Henzel WJ, Shillinglaw W, Li S & Cao Z MyD88: an adapter that recruits IRAK to the IL-1 receptor complex. Immunity 7, 837–847 (1997). [PubMed: 9430229]
36. Guo Y et al. Tim50, a component of the mitochondrial translocator, regulates mitochondrial integrity and cell death. J Biol Chem 279, 24813–24825 (2004). [PubMed: 15044455]
37. Rehling P, Brandner K & Pfanner N Mitochondrial import and the twin-pore translocase. Nat Rev Mol Cell Biol 5, 519–530 (2004). [PubMed: 15232570]
38. Saitoh T et al. Tom20 recognizes mitochondrial presequences through dynamic equilibrium among multiple bound states. EMBO J 26, 4777–4787 (2007). [PubMed: 17948058]
39. Abe Y et al. Structural basis of presequence recognition by the mitochondrial protein import receptor Tom20. Cell 100, 551–560 (2000). [PubMed: 10721992]
40. Lee CM, Sedman J, Neupert W & Stuart RA The DNA helicase, Hmi1p, is transported into mitochondria by a C-terminal cleavable targeting signal. J Biol Chem 274, 20937–20942 (1999). [PubMed: 10409639]

41. Franconi F et al. Are the available experimental models of type 2 diabetes appropriate for a gender perspective? Pharmacol Res 57, 6–18 (2008). [PubMed: 18221886]
42. Kautzky-Willer A, Harreiter J & Pacini G Sex and Gender Differences in Risk, Pathophysiology and Complications of Type 2 Diabetes Mellitus. Endocr Rev 37, 278–316 (2016). [PubMed: 27159875]
43. Cypess AM et al. Identification and importance of brown adipose tissue in adult humans. N Engl J Med 360, 1509–1517 (2009). [PubMed: 19357406]
44. Nijtmans LG, Artal SM, Grivell LA & Coates PJ The mitochondrial PHB complex: roles in mitochondrial respiratory complex assembly, ageing and degenerative disease. Cell Mol Life Sci 59, 143–155 (2002). [PubMed: 11852914]
45. Glytsou C et al. Optic Atrophy 1 Is Epistatic to the Core MICOS Component MIC60 in Mitochondrial Cristae Shape Control. Cell Rep 17, 3024–3034 (2016). [PubMed: 27974214]
46. Del Dotto V et al. OPA1 Isoforms in the Hierarchical Organization of Mitochondrial Functions. Cell Rep 19, 2557–2571 (2017). [PubMed: 28636943]
47. Sun XJ et al. Deletion of interleukin 1 receptor-associated kinase 1 (Irak1) improves glucose tolerance primarily by increasing insulin sensitivity in skeletal muscle. J Biol Chem 292, 12339–12350 (2017). [PubMed: 28572512]
48. Rosselin M, Santo-Domingo J, Bermont F, Giacomello M & Demaurex N L-OPA1 regulates mitoflash biogenesis independently from membrane fusion. EMBO Rep 18, 451–463 (2017). [PubMed: 28174208]
49. Jian C et al. Deficiency of PHB complex impairs respiratory supercomplex formation and activates mitochondrial flashes. J Cell Sci 130, 2620–2630 (2017). [PubMed: 28630166]
50. Galmozzi A et al. ThermoMouse: an in vivo model to identify modulators of UCP1 expression in brown adipose tissue. Cell Rep 9, 1584–1593 (2014). [PubMed: 25466254]
51. Frezza C, Cipolat S & Scorrano L Organelle isolation: functional mitochondria from mouse liver, muscle and cultured fibroblasts. Nat Protoc 2, 287–295 (2007). [PubMed: 17406588]
52. Huynh FK, Green MF, Koves TR & Hirschey MD Measurement of fatty acid oxidation rates in animal tissues and cell lines. Methods Enzymol 542, 391–405 (2014). [PubMed: 24862277]
53. Han Z et al. Shear-induced reactive nitrogen species inhibit mitochondrial respiratory complex activities in cultured vascular endothelial cells. Am J Physiol Cell Physiol 292, C1103–1112 (2007). [PubMed: 17020931]
54. Chen YR, Chen CL, Pfeiffer DR & Zweier JL Mitochondrial complex II in the post-ischemic heart: oxidative injury and the role of protein S-glutathionylation. J Biol Chem 282, 32640–32654 (2007). [PubMed: 17848555]
55. Yeh ST et al. Preservation of mitochondrial function with cardiopulmonary resuscitation in prolonged cardiac arrest in rats. J Mol Cell Cardiol 47, 789–797 (2009). [PubMed: 19751739]
56. Felgner PL, Messer JL & Wilson JE Purification of a hexokinase-binding protein from the outer mitochondrial membrane. J Biol Chem 254, 4946–4949 (1979). [PubMed: 447625]
57. Sottocasa GL, Kuylenstierna B, Ernster L & Bergstrand A An electron-transport system associated with the outer membrane of liver mitochondria. A biochemical and morphological study. J Cell Biol 32, 415–438 (1967). [PubMed: 10976232]
58. Pagliarini DJ et al. Involvement of a mitochondrial phosphatase in the regulation of ATP production and insulin secretion in pancreatic beta cells. Mol Cell 19, 197–207 (2005). [PubMed: 16039589]

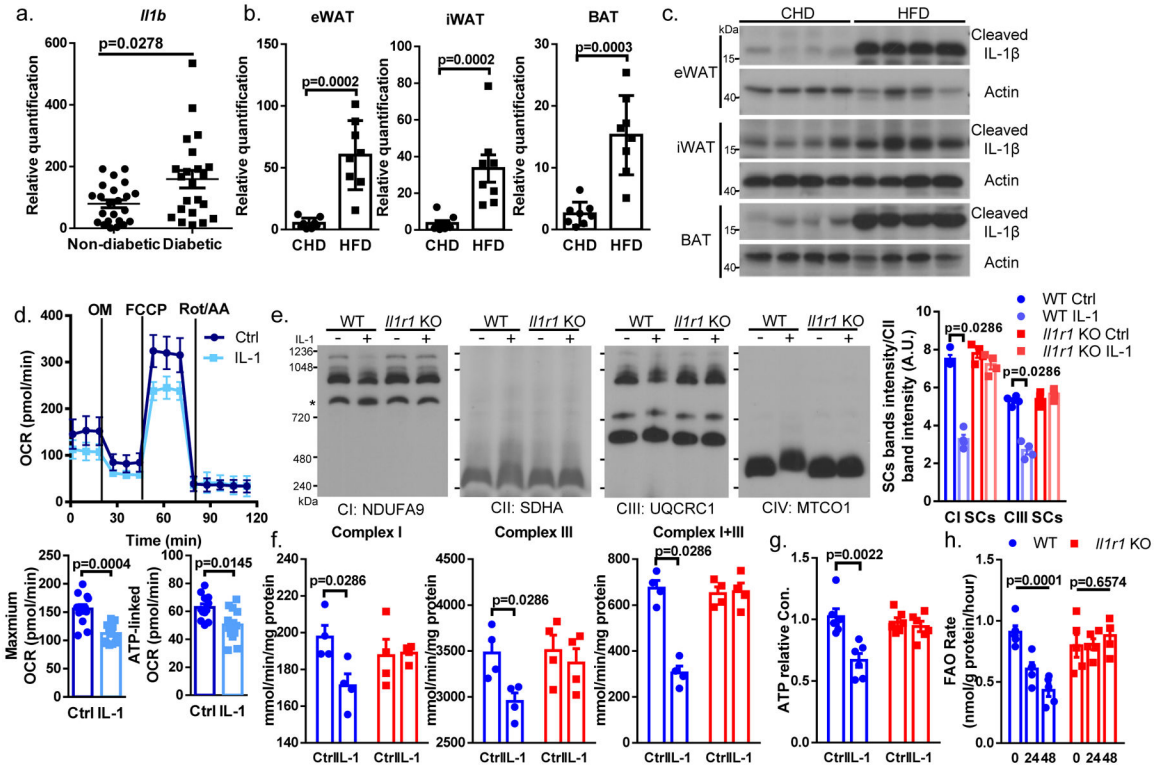

Figure 1. IL-1β inhibits mitochondrial oxidative phosphorylation and super-complex formation in adipocytes.

a. *Il1b* mRNA expression in human non-diabetic (n=24) and diabetic (n=22) omental adipose tissue. **b.** *Il1b* mRNA expression in epididymal white adipose tissue (eWAT), inguinal WAT (iWAT) and interscapular brown adipose tissue (BAT) from chow diet-fed (CHD) and high fat diet-fed (HFD) mice (n=8 mice for each group). **c.** Western blot of cleaved IL-1β in whole eWAT, iWAT and BAT tissue lysates from CHD and HFD mice. **d.** O_2 consumption rate (OCR) in newly differentiated primary adipocytes treated with or without IL-1β for 24 hours. Data represent mean ± SEM. Data represent one of five independent experiments with similar results. Maximal Respiratory Capacity and ATP-linked OCR are shown as bar graphs (n=12 biological independent samples). **e.** Mitochondrial proteins were extracted from WT and *Il1r1* KO newly differentiated primary adipocytes treated with or without IL-1β for 24 hours and analyzed by BN-PAGE, followed by western blot analysis with indicated antibodies. Data represent one of five independent experiments with similar results. For quantification of super-complex, the signals corresponding to bands above free complex I (starred) were used and normalized to signals from Complex II (n=4 biological independent samples). **f.** The activities of respiratory complexes in the isolated mitochondria from WT and *Il1r1* KO newly adipocytes were treated with or without IL-1β (n=4 biological independent samples). **g.** Cellular ATP level in WT and *Il1r1* KO newly adipocytes were treated with or without IL-1β (n=6 biological independent samples). **h.** [1-^{14}C]-palmitic acid oxidation-rate in mitochondria from WT and *Il1r1* KO newly differentiated primary adipocytes treated with or without IL-1β (n=5 biological independent samples). **a, b, d, e, f, g**: Student's t-test (two-tailed) was performed. Data represent mean ± SEM. **h**, one-way ANOVA was performed. Data represent mean ±

SEM. The experiments were repeated for five times with similar results. Data represent mean ± SEM, *: $p<0.05$.

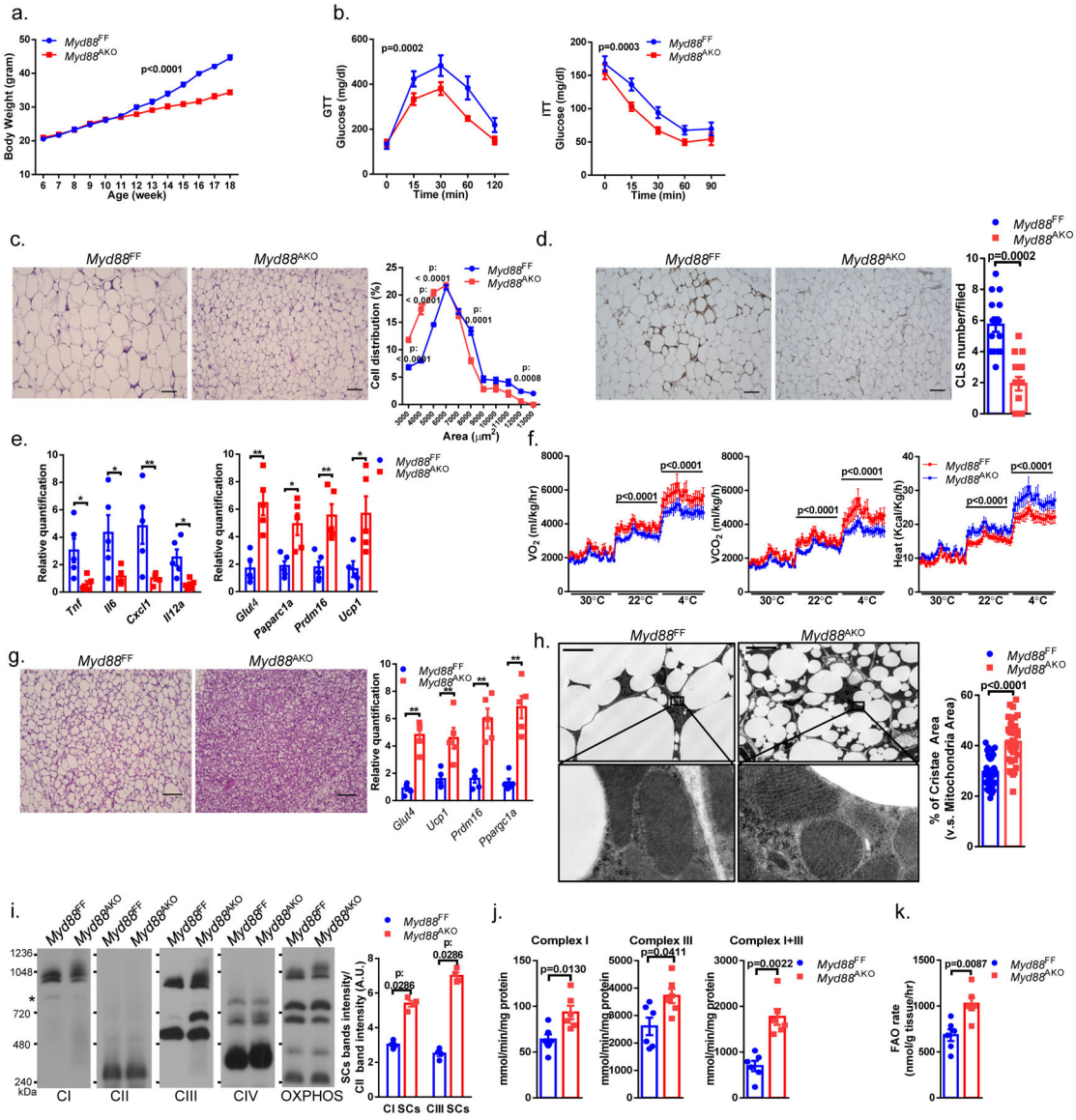

Figure 2. Adipocyte-specific MyD88 deficiency (*Myd88*^{AKO}) improves HFD-induced obesity and energy expenditure.

a. Body weight of *Myd88*^{FF} and *Myd88*^{AKO} mice on HFD feeding (n=7males per group). **b.** Glucose tolerance test (GTT) and insulin tolerance test (ITT) were performed on HFD-fed of *Myd88*^{FF} and *Myd88*^{AKO} mice (n=6 mice). **c.** H&E staining of iWAT sections from HFD-fed of *Myd88*^{FF} and *Myd88*^{AKO} mice. Cell size was quantified (3 views per slide, 3 sections per mouse, n=5). **d.** Mac2 staining of iWAT sections from HFD-fed mice. Crown-like structures (CLS) were quantified via Mac2 staining. (3 views per slide, 3 sections per mouse, n=5 mice). **e.** Expression of indicated mRNAs in iWAT from HFD-fed mice (n=5). *: p<0.05. **: p<0.01. **f.** Quantification of $\dot{V}O_2$, VCO_2 levels and heat production by HFD-fed mice were measured using indirect calorimetry methods (n=5 mice). **g.** H&E staining of BAT sections and expression of indicated mRNAs in BAT from HFD-fed mice (n=5). **: p<0.01. **c, d, g**: scale bars, 150 μm. **h.** Transmission electron microscopy analysis of BAT sections from HFD-fed mice. scale bars, 1 μm. Morphometric analysis of cristae area versus

mitochondria area in 40 randomly selected mitochondria per group. **i.** Mitochondrial proteins were extracted from BAT of HFD-fed mice and analyzed by BN-PAGE, followed by western blot analysis with indicated antibodies. Data represent one of five independent experiments with similar results. For quantification of super-complex, the signals corresponding to bands above free complex I (starred) were used and normalized to signals from Complex II (n=4 biological independent samples). **j.** The activities of respiratory complexes in the isolated mitochondria from BAT of HFD-fed $MyD88^{FF}$ and $MyD88^{AKO}$ (n=6 biological independent samples). **k.** [1-^{14}C]-palmitic acid oxidation-rate in mitochondria from BAT of HFD-fed mice (n=6 biological independent samples). **a, b, f**: Two-way ANOVA, followed by post hoc analysis was performed. Data represent mean ± SEM. **c, d, e, g, h, i, j, k**: Student's t-test (two-tailed) was performed. Data represent mean ± SEM.

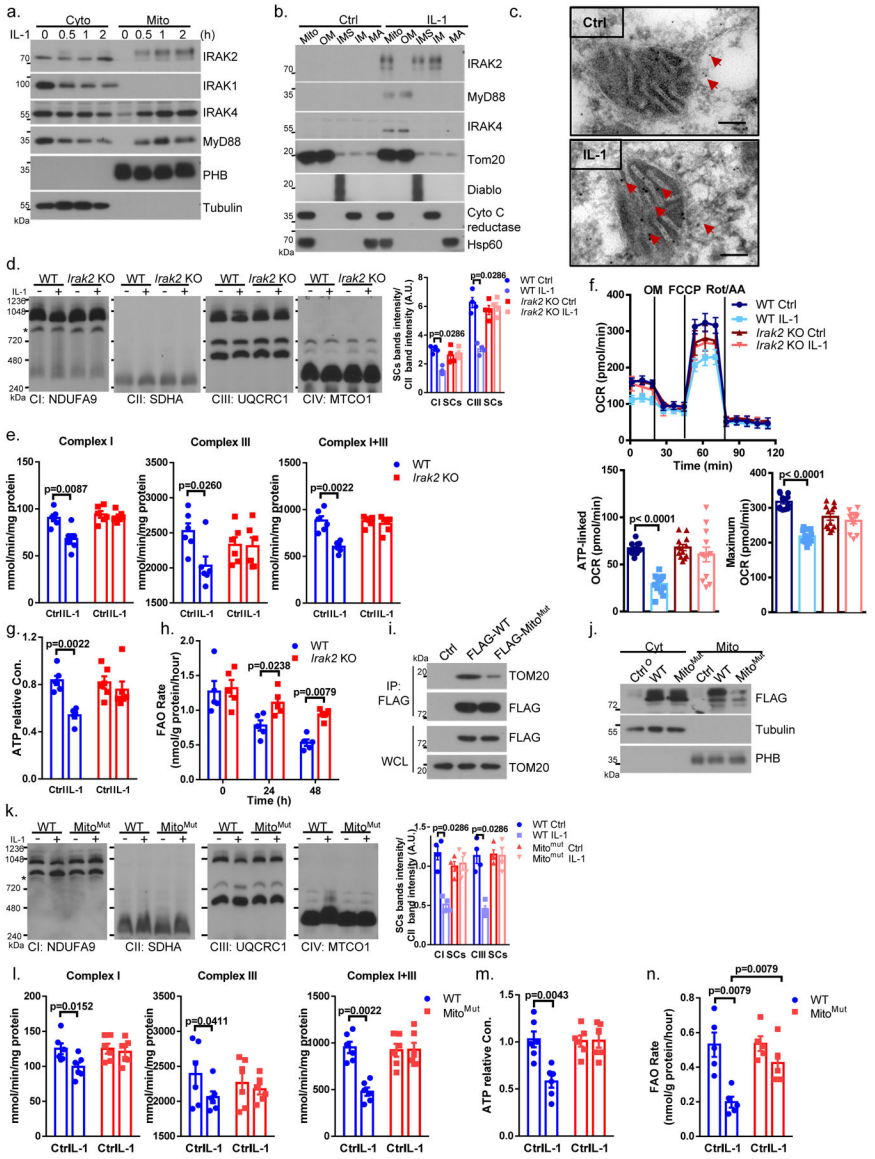

Figure 3. IL-1β induces translocation of IRAK2 into inner mitochondrial membrane to suppress oxidative phosphorylation and fatty acid oxidation.

a. Western blot analysis of cytoplasmic (Cyto) and mitochondrial (Mito) proteins from IL-1β treated newly differentiated primary adipocytes. Data represent one of five independent experiments with similar results. **b.** Western blot analysis of proteins of mitochondria (Mito), outer mitochondrial membrane (OM), inter mitochondrial membrane space (IMS), inner mitochondrial membrane (IM) and mitochondrial matrix (MA) from IL-1β treated newly differentiated primary adipocytes mitochondrial. Data represent one of five independent experiments with similar results. **c.** Immunogold staining of HA-tagged IRAK2 in newly differentiated primary adipocytes from *Irak2*-HA reporter mice with or without IL-1β treatment for 24h. Scale bars, 200 nm. **d.** Mitochondrial proteins were extracted from WT and *Irak2* KO newly differentiated primary adipocytes treated with or without IL-1β for indicated time points and analyzed by BN-PAGE, followed by western blot analysis with indicated cocktail antibodies. Data represent one of five independent

experiments with similar results. For quantification of super-complex, the signals corresponding to bands above free complex I (starred) were used and normalized to signals from Complex II (n=4 biological independent samples). **e.** The activities of respiratory complexes in the isolated mitochondria from WT and *Irak2* KO newly adipocytes were treated with or without IL-1β (n=6 biological independent samples). **f.** O_2 consumption rate (OCR) in newly differentiated primary adipocytes treated with or without IL-1β for 24 hours. Data represent one of five independent experiments with similar results. Maximal Respiratory Capacity and ATP-linked OCR are shown as bar graphs (n=12 biological independent samples). **g.** Cellular ATP level in WT and *Irak2* KO newly adipocytes were treated with or without IL-1β (n=6 biological independent samples). h. [1-^{14}C]-palmitic acid oxidation-rate in mitochondria from WT and IL-1R1 KO newly differentiated primary adipocytes treated with or without IL-1β (n=5 biological independent samples). **i-n.** Flag-tagged wild-type and IRAK2 mito-mutant were restored in *Irak2* KO adipocytes. (i) Co-immunoprecipitation (IP) analysis of Flag in whole cell lysates (WCL) and followed by western blot analysis. (L) Western blot analysis of cytoplasmic (Cyto) and mitochondrial (Mito) proteins. (M) Mitochondrial proteins were extracted followed by western blot analysis with indicated cocktail antibodies. Data represent one of five independent experiments with similar results. For quantification of super-complex, the signals corresponding to bands above free complex I (starred) were used and normalized to signals from Complex II (n=4 biological independent samples). (l) The activities of respiratory complexes in the isolated mitochondria were treated with or without IL-1β (n=6 biological independent samples) (m) Cellular ATP level (n=6 biological independent samples) and (n) [1-^{14}C]-palmitic acid oxidation-rate in mitochondria(K) (n=5 biological independent samples). **d, e, f, g, h, k, l, m, n**: Student's t-test (two-tailed) was performed. Data represent mean ± SEM.

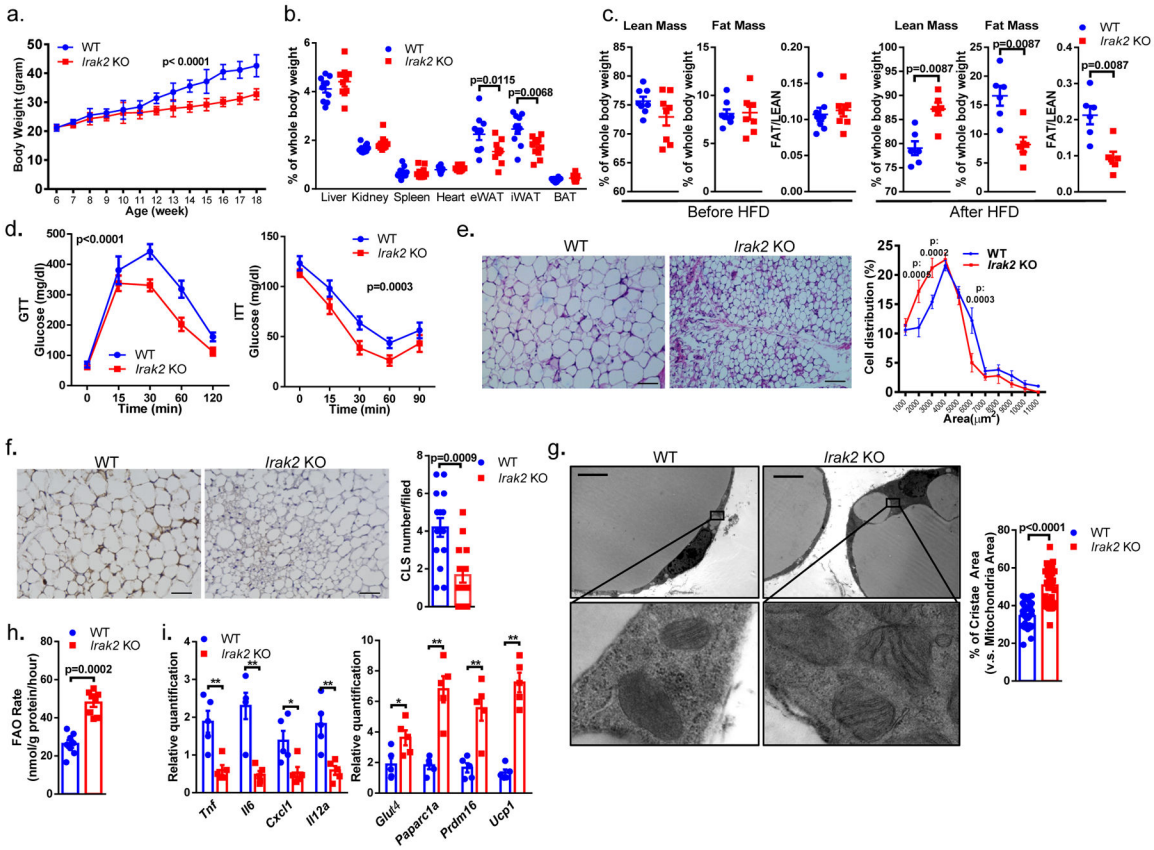

Figure 4. IRAK2 deficiency improves HFD-induced obesity and energy expenditure.

a. Body weight of WT and *Irak2* KO mice on HFD feeding (n=6 males per group). **b.** Indicated organs were isolated from HFD-fed WT and *Irak2* KO mice. The percentages to whole body weight were blotted (n=10). **c.** EchoMRI analysis of WT and *Irak2* KO mice before and after HFD feeding (n=8). **d.** Glucose tolerance test (GTT) and insulin tolerance test (ITT) were performed on HFD-fed of WT and *Irak2* KO mice (n=8 males per group). **e.** H&E staining of iWAT sections from HFD-fed of WT and *Irak2* KO mice. Cell size was quantified (3 views per slide, 3 sections per mouse, n=5). **f.** Mac2 staining of iWAT sections from HFD-fed mice. Crow-like structure (CLS) was quantified (3 views per slide, 3 sections per mouse, n=5). **e, f**: scale bars, 150 μm. **g.** Transmission electron microscopy analysis of iWAT from WT and *Irak2* KO HFD mice. scale bars, 1 μm. Morphometric analysis of cristae area versus mitochondria area in 40 randomly selected mitochondria per group. **h.** [1-^{14}C]-palmitic acid oxidation-rate in mitochondria from iWAT of HFD-fed mice (n=8 biological independent samples). **i.** Expression of indicated mRNAs in iWAT from HFD-fed mice (n=6 biological independent samples). *: p<0.05. **: p<0.01. **a, d**: Two-way ANOVA, followed by post hoc analysis was performed. Data represent mean ± SEM. **b, c, e, f, g, h, i**: Student's t-test (two-tailed) was performed. Data represent mean ± SEM.

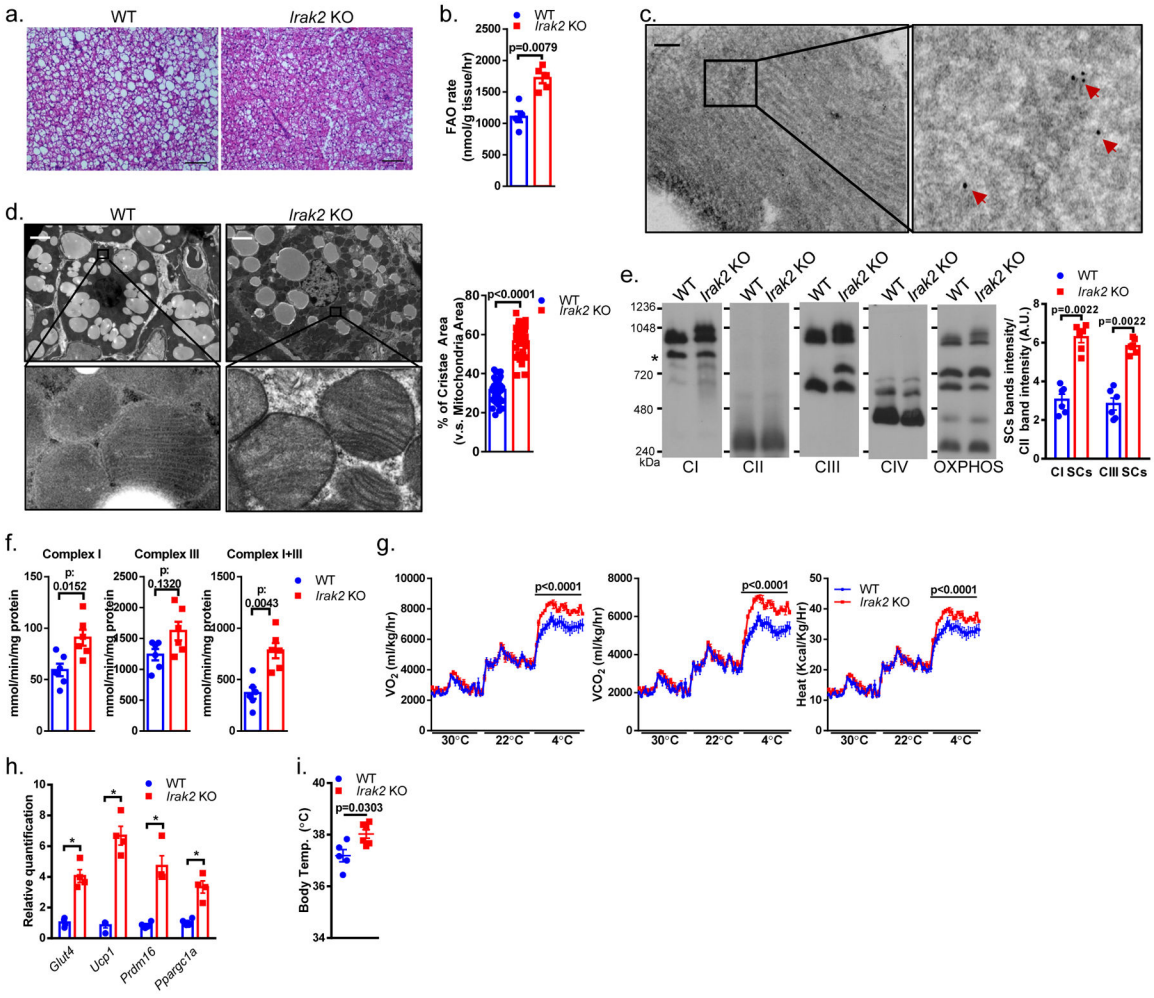

Figure 5. IRAK2 deficiency prevents HFD-induced BAT dysfunction.

a. H&E staining of BAT sections from HFD-fed mice. scale bars, 150 μm. **b.** [1-^{14}C]-palmitic acid oxidation-rate in mitochondria from BAT of HFD-fed mice (n=5 biological independent samples). **c.** Immunogold staining of HA-tagged IRAK2 in BAT sections of HFD-fed *Irak2*-HA reporter mice. scale bars, 200 nm. **d.** Transmission electron microscopy analysis of BAT sections from HFD-fed mice. scale bars, 3 nm. Morphometric analysis of cristae area versus mitochondria area in 40 randomly selected mitochondria per group. **e.** Mitochondrial proteins were extracted from BAT of HFD-fed mice and analyzed by BN-PAGE, followed by western blot analysis with indicated antibodies. For quantification of super-complex, the signals corresponding to bands above free complex I (starred) were used and normalized to signals from Complex II (n=6 biological independent samples). **f.** The activities of respiratory complexes in the isolated mitochondria from BAT of HFD-fed WT and IRAK2 mice (n=6 biological independent samples). **g.** Quantification of $\dot{V}O_2$, VCO_2 levels and heat production by HFD-fed WT and IRAK2 KO mice were measured using indirect calorimetry methods (n=5). **h.** Expression of indicated mRNAs in BAT from HFD-fed mice (n=5). **i.** Rectal temperatures were measured for HFD-fed WT and IRAK2 KO HFD mice. (n=4). *: p<0.05. **b, d, e, f, h, i**: Student's t-test (two-tailed) was performed. Data

represent mean ± SEM. **g**: Two-way ANOVA, followed by post hoc analysis was performed. Data represent mean ± SEM.

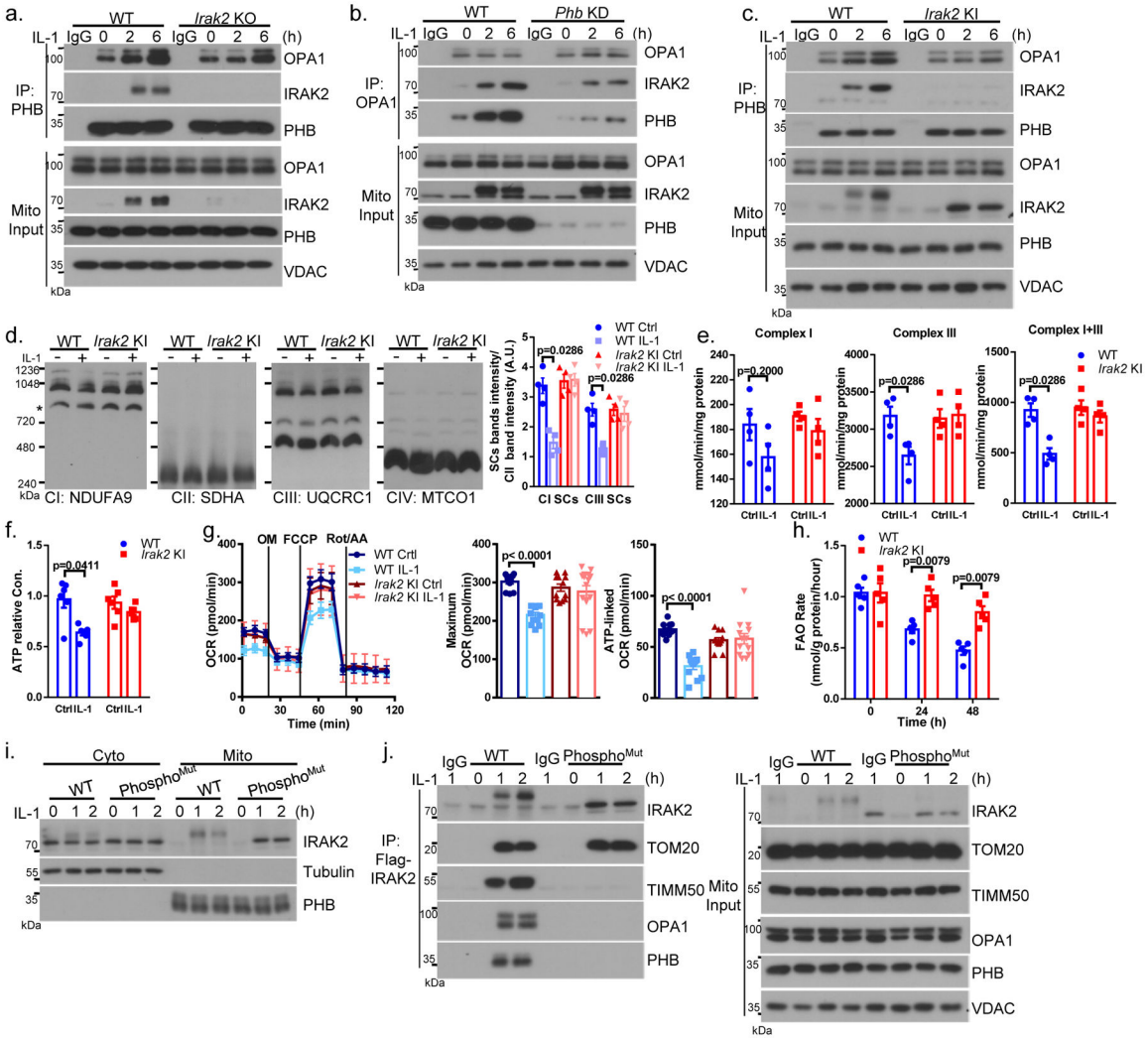

Figure 6. IRAK2 disrupts mitochondrial respiratory chain super-complex formation via interaction with PHB-OPA1.

a. Co-immunoprecipitation (IP) analysis of PHB in mitochondria of WT and *Irak2* KO newly differentiated primary adipocytes treated with IL-1β for indicated time points and followed by western blot analysis. **b.** Co-immunoprecipitation (IP) analysis of OPA1 in mitochondria of non-targeting siRNA (Ctrl) and PHB siRNA transfected (*Phb* KD) primary adipocytes treated with IL-1β for indicated time points and followed by western blot analysis. **c.** Co-immunoprecipitation (IP) analysis of PHB in mitochondria of WT and *Irak2* KI newly differentiated primary adipocytes treated with IL-1β for indicated time points and followed by western blot analysis. **a, b, c**: Data represent one of five independent experiments with similar results. **d.** Mitochondrial proteins were extracted WT and *Irak2* KI newly differentiated primary adipocytes treated with IL-1β for indicated time points and analyzed by BN-PAGE, followed by Western blot analysis with indicated antibodies. Data represent one of five independent experiments with similar results. For quantification of super-complex, the signals corresponding to bands above free complex I (starred) were used and normalized to signals from Complex II (n=4 biological independent samples). **e.** The

activities of respiratory complexes in the isolated mitochondria from WT and *Irak2* KI newly adipocytes were treated with or without IL-1β (n=4 biological independent samples). **f**. Cellular ATP level in WT and *Irak2* KI newly adipocytes were treated with or without IL-1β (n=6 biological independent samples). **g.** O_2 consumption rate (OCR) in newly differentiated primary adipocytes treated with or without IL-1β for 24 hours. Data represent one of five independent experiments with similar results. Maximal Respiratory Capacity and ATP-linked OCR are shown as bar graphs. Maximal Respiratory Capacity and ATP-linked OCR are shown as bar graphs (n=12 biological independent samples). **h.** [1-^{14}C]-palmitic acid oxidation-rate in mitochondria from WT and IRAK2 KI primary adipocytes treated with IL-1β for indicated time points (n=6 biological independent samples). **i-j.** Flag-tagged wild-type and IRAK2 phospho-mutant were restored in *Irak2* KO adipocytes. (K) Western blot analysis of cytoplasmic and mitochondrial proteins. (L) Co-immunoprecipitation (IP) analysis of Flag in whole cell lysates and followed by western blot analysis. The experiments were repeated for five times with similar results. **d, e, f, g, h**: Student's t-test (two-tailed) was performed. Data represent mean ± SEM.

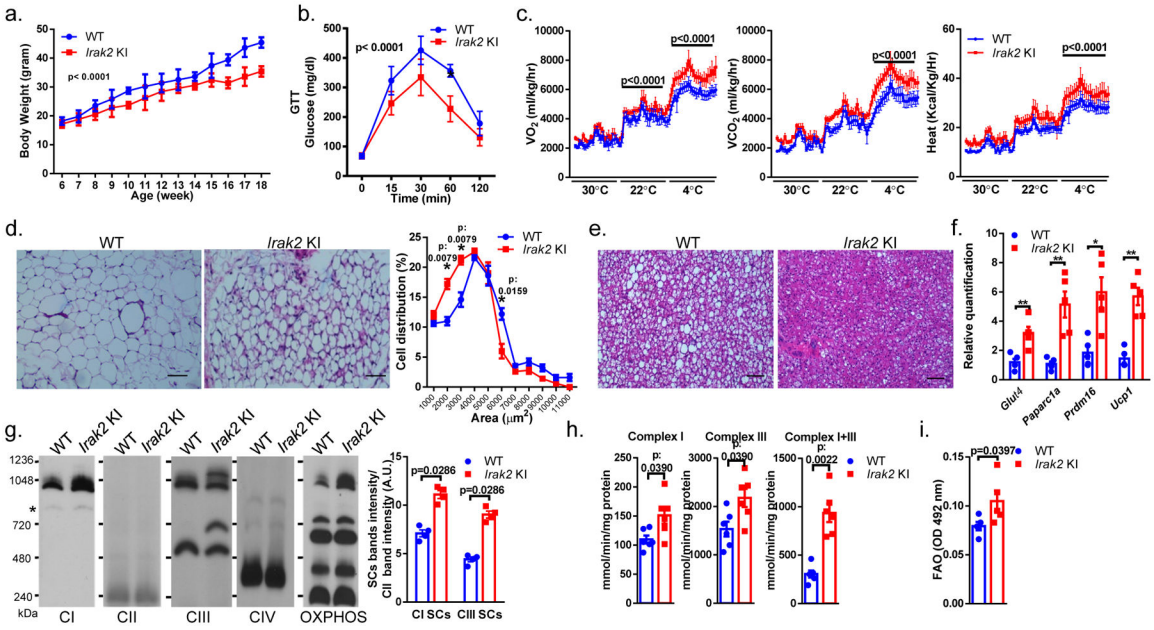

Figure 7. IRAK2 kinase activity contributes to HFD-induced obesity and BAT dysfunction.

a. Body weight of WT (n=7 males) and *Irak2* KI mice on HFD feeding (n=9 males). **b.** Glucose tolerance test (GTT) was performed on HFD-fed of WT and *Irak2* KI mice (n=5 males). **c.** Quantification of $\dot{V}O_2$, VCO_2 levels and heat production by HFD-fed WT and *Irak2* KI mice were measured using indirect calorimetry methods (n=5). **d.** H&E staining of iWAT sections from HFD-fed of *Irak2* KI and control mice. Cell size was quantified (3 views per slide, 3 sections per mouse, n=5). **e.** H&E staining of BAT sections from HFD-fed mice**. d,e**: scale bars, 150 μm. **f.** Expression of indicated mRNAs in BAT from HFD-fed mice (n=5). *: p<0.05. **: p<0.01. **g**. Mitochondrial proteins were extracted from BAT of HFD-fed mice and analyzed by BN-PAGE, followed by western blot analysis with indicated antibodies. For quantification of super-complex, the signals corresponding to bands above free complex I (starred) were used and normalized to signals from Complex II (n=4 biological independent samples). **h.** The activities of respiratory complexes in the isolated mitochondria from BAT of HFD-fed WT and *Irak2* KI mice (n=6). **i.** Octanoyl-carnitine oxidation-rate in isolated mitochondria from BAT of HFD-fed mice with indicated genotypes (n=5 biological independent samples). **a, b, c**: Two-way ANOVA, followed by post hoc analysis was performed. Data represent mean ± SEM. **d, f, g, h, i**: Student's t-test (two-tailed) was performed. Data represent mean ± SEM.

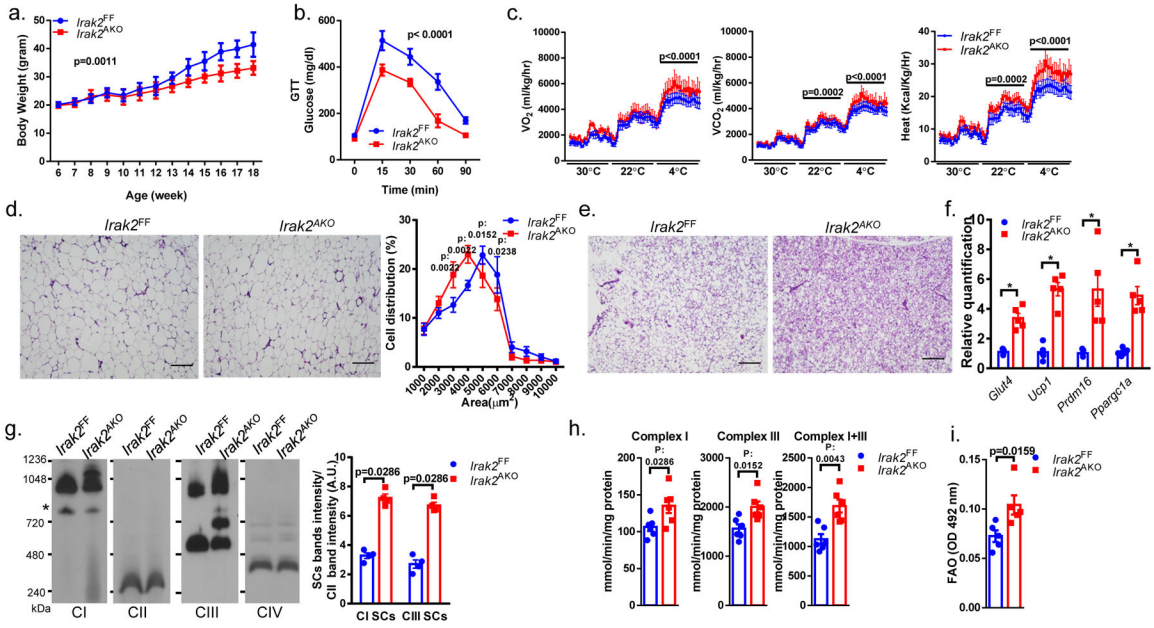

Figure 8. Adipocyte-specific IRAK2 contributes to HFD-induced obesity and BAT dysfunction.

a. Body weight of *Irak2*^{FF} (n=7 males) and *Irak2*^{AKO} mice on HFD feeding (n=6 males). **b.** Glucose tolerance test (GTT) was performed on HFD-fed of *Irak2*^{FF} and *Irak2*^{AKO} mice (n=6 males). **c.** Quantification of $\dot{V}O_2$, VCO_2 levels and heat production by HFD-fed *Irak2*^{FF} (n=6) and *Irak2*^{AKO} mice were measured using indirect calorimetry methods (n=5). **d.** H&E staining of iWAT sections from HFD-fed *Irak2*^{AKO} and control mice. Cell size was quantified (3 views per slide, 3 sections per mouse, n=5). **e.** H&E staining of BAT sections from HFD-fed mice**. d,e**: scale bars, 150 μm. **f.** Expression of indicated mRNAs in BAT from HFD-fed mice (n=5). *: p<0.05. **g**. Mitochondrial proteins were extracted from BAT of HFD-fed mice and analyzed by BN-PAGE, followed by western blot analysis with indicated antibodies. For quantification of super-complex, the signals corresponding to bands above free complex I (starred) were used and normalized to signals from Complex II (n=4 biological independent samples). **h.** The activities of respiratory complexes in the isolated mitochondria from BAT of HFD-fed *Irak2*^{FF} and *Irak2*^{AKO} mice (n=6). **i.** Octanoyl-carnitine oxidation-rate in isolated mitochondria from BAT of HFD-fed mice with indicated genotypes (n=5 biological independent samples). **a, b, c**: Two-way ANOVA, followed by post hoc analysis was performed. Data represent mean ± SEM. **d, f, g, h, i**: Student's t-test (two-tailed) was performed. Data represent mean ± SEM.